

**INTERACTIONS OF CANCER CELLS AND
MACROPHAGES ON THE EGF-EGFR AXIS:
CHEMOTAXIS, HAPTOTAXIS OR DIRECT
CONTACT?**

**A Thesis Submitted to
The Graduate School of Engineering and Sciences of
İzmir Institute of Technology
in Partial Fulfillment of the Requirements for the Degree of**

MASTER OF SCIENCE

in Biotechnology and Bioengineering

**by
Sevgi ÖNAL**

**June 2017
İZMİR**

We approve the thesis of **Sevgi ÖNAL**

Examining Committee Members:

Assoc. Prof. Dr. Devrim PESEN OKVUR

Department of Molecular Biology and Genetics, Izmir Institute of Technology

Assist. Prof. Dr. Özden YALÇIN ÖZUYSAL

Department of Molecular Biology and Genetics, Izmir Institute of Technology

Prof. Dr. Esra ERDAL

Department of Medical Biology and Genetics & Izmir International Biomedicine and Genome Institute, Dokuz Eylul University

02 June 2017

Assoc. Prof. Dr. Devrim PESEN OKVUR

Supervisor, Department of Molecular Biology and Genetics, Izmir Institute of Technology

Prof. Dr. Volga BULMUŞ

Co-Supervisor, Department of Bioengineering, Izmir Institute of Technology

Assoc. Prof. Dr. Engin ÖZÇİVİCİ

Head of the Department of Biotechnology and Bioengineering

Prof. Dr. Aysun SOFUOĞLU

Dean of the Graduated School of Engineering and Sciences

ACKNOWLEDGMENTS

I would like to thank my supervisor Assoc. Prof. Dr. Devrim PESEN OKVUR for her training, encouragement, understanding, guidance and support throughout this study and the rest of my education since 2012.

I am thankful to my co-supervisor Prof. Dr. Volga BULMUŞ and the members of my thesis defense committee Assist. Prof. Dr. Özden YALÇIN ÖZUYSAL and Prof. Dr. Esra ERDAL.

This work was supported by FP7 Marie Curie Grant number PIRG08-GA-2010-27697 and IYTE Scientific Research Project Grant number 2011IYTE25 (to D. Pesen Okvur). Cell-on-a-chips were fabricated at the IYTE Applied Quantum Research Center, supported by DPT (State Planning Organization) Grant 2009K120860.

I thank Assoc. Prof. Dr. Alper ARSLANOĞLU, Assoc. Prof. Dr. Engin ÖZÇİVİCİ and Biotechnology and Bioengineering Application and Research Center for access to fluorescence microscopes, also Prof. Dr. Ahmet KOÇ for access to UV/Vis Spectrophotometer.

I would like to express my deepest appreciation and thanks to the current members and alumni of the Controlled *in vitro* Microenvironments (CivM) Laboratory for their team spirit and support, especially Merve TÜRKER for her significant contributions to the completion of the study, and Hamdullah YANIK, Gizem BATI, Berrin ÖZDİL, Tuğçe ORUÇ, Murat SAĞLAM, Emre TARIM, Nurullah SATI, Muhammed ÖZBULUT, Müge BİLGİN, Begüm GÖKÇE, Yeşim ŞİRİN and İsmail TAHMAZ.

Finally, I would like to express my greatest love, appreciation and countless thanks to my family for their encouragement, understanding, help and support during my whole life. Without their love, there would be no way for my success.

ABSTRACT

INTERACTIONS OF CANCER CELLS AND MACROPHAGES ON THE EGF-EGFR AXIS: CHEMOTAXIS, HAPTOTAXIS OR DIRECT CONTACT?

Breast cancer cells (BCC) and macrophages are known to interact via epidermal growth factor (EGF) produced by macrophages and colony stimulating factor-1 (CSF-1) produced by BCC. Despite contradictory findings, this interaction is perceived as a paracrine loop. Yet, the underlying mechanism of interaction remains unclear. Here, we investigated interactions of BCC with macrophages in 2D and 3D. BCC did not show chemotaxis to macrophages in custom designed 3D cell-on-a-chip devices, which was in agreement with ELISA results showing that macrophage-derived-EGF was not secreted into macrophage-conditioned-medium. Live cell imaging of BCC in the presence and absence of iressa showed that macrophages but not macrophage-derived-matrix modulated adhesion and motility of BCC in 2D. 3D co-culture experiments in matrigel and collagen showed that BCC changed their multicellular organization in the presence of macrophages. In custom designed 3D co-culture cell-on-a-chip devices, macrophages reduced and promoted migration of BCC in matrigel and collagen, respectively. Furthermore, adherent but not suspended BCC endocytosed EGFR when in contact with macrophages. Collectively, our data revealed that macrophages showed chemotaxis towards BCC-derived-CSF-1 whereas BCC required direct contact to interact with macrophage-derived-EGF. We propose that the interaction between cancer cells and macrophages is a paracrine-juxtacrine loop of CSF-1 and EGF, respectively.

Keywords and Phrases: breast cancer, epidermal growth factor, macrophage colony stimulating factor-1, paracrine signaling, juxtacrine signaling, chemotaxis, lab-on-a-chip, three dimensional cell culture

ÖZET

EGF-EGFR EKSENİNDE KANSER HÜCRELERİ VE MAKROFAJLARIN ETKİLEŞİMLERİ: KEMOTAKSİS, HAPTOTAKSİS YA DA DİREKT TEMAS?

Meme kanseri hücreleri (MKH) ve makrofajların, makrofajlar tarafından üretilen epidermal büyüme faktörü (EBF) ve MKH tarafından üretilen koloni uyarıcı faktör-1 (KUF-1) aracılığıyla etkileşime girdiği bilinmektedir. Çelişkili bulgulara rağmen, bu etkileşim parakrin döngü olarak algılanır. Bununla birlikte, etkileşimin altında yatan mekanizma belirsizliğini koruyor. Burada, MKH'nin makrofajlarla etkileşimlerini 2 boyutta (2B) ve 3 boyutta (3B) araştırdık. MKH, makrofaj türevli EBF'nin makrofaj-koşullandılmış-ortama salgılanmadığını gösteren ELISA sonuçlarına uygun olarak, özel olarak tasarlanmış 3B yonga-üstü-hücre cihazlarında makrofajlara kemotaksis göstermedi. Iressa varlığında ve yokluğunda MKH'nin canlı hücre görüntülemesi, makrofajların MKH'nin adezyon ve motilitesini modüle ettiğini, makrofaj türevli matriksin ise etmediğini gösterdi. Matrigel ve kollajendeki 3B ortak kültür deneyleri, makrofajların varlığında, MKH'nin çok hücreli organizasyonunu değiştirdiğini gösterdi. Özel olarak tasarlanmış 3B yonga-üstü-hücre ortak kültür cihazlarında, makrofajlar sırasıyla matrigel ve kollajendeki MKH'nin migrasyonunu azalttı ve yükseltti. Ayrıca, makrofajlarla temas halinde, asılı MKH etmezken yapışık MKH EBF reseptörünü endositize etti. Toplu olarak, verilerimiz makrofajların MKH türevli KUF-1'e karşı kemotaksis gösterdiğini, buna karşılık MKH'nin makrofaj kaynaklı EBF ile etkileşime girmesi için doğrudan temasa ihtiyaç duyduğunu ortaya koydu. Kanser hücreleri ile makrofajlar arasındaki etkileşimin sırasıyla KUF-1 ve EBF'nin bir parakrin-jukstakrin halkası olduğunu önermekteyiz.

Anahtar Kelimeler ve Deyimler: meme kanseri, epidermal büyüme faktörü, makrofaj koloni stimulan faktör-1, parakrin sinyalizasyon, junkstakrin sinyalizasyon, kemotaksis, yonga-üstü-laboratuvar, üç boyutlu hücre kültürü

To my family...

TABLE OF CONTENTS

LIST OF FIGURES	ix
LIST OF TABLES.....	x
CHAPTER 1. INTRODUCTION	1
CHAPTER 2. MATERIALS AND METHODS	6
2.1. Cell Culture.....	6
2.2. Cell-on-a-chip Experiments	6
2.3. Protein Quantification and ELISA.....	7
2.4. Live Cell Imaging	7
2.5. 3D Co-culture Hydrogel Experiments	8
2.6. Endocytosis in Suspended Cells	9
2.7. Endocytosis in Adherent Cells.....	10
2.8. Image Analysis.....	10
2.9. Statistical Analysis and Data Presentation.....	10
CHAPTER 3. RESULTS AND DISCUSSION.....	11
3.1. BCC cells did not show chemotaxis towards macrophages whereas macrophages showed chemotaxis towards BCC.....	11
3.1.1. ELISA Results.....	13
3.2. Macrophages but not macrophage-derived-matrix modulated adhesion and motility of BCC in an EGF-dependent manner	14
3.2.1. Snapshots from 5 hours Long Live Cell Imaging at every 15 min	19
3.3. Co-culture of BCC with Macrophages in Hydrogel Drops or in Cell- on-a-chips	25
3.3.1. Co-culture of BCC with macrophages in matrigel or collagen hydrogel drops changed their multicellular organization	25
3.3.2. Macrophages reduced and promoted migration of BCC in matrigel and collagen, respectively.....	30

3.4. Adherent but not suspended BCC endocytosed EGFR when in contact with macrophages.....	31
CHAPTER 4. CONCLUSION	36
REFERENCES	37
APPENDICES	
APPENDIX A. PUBLISHED ARTICLE.....	43
APPENDIX B. SUPPLEMENTARY VIDEOS	44
APPENDIX C. SUPPLEMENTARY DATASET.....	45

LIST OF FIGURES

<u>Figure</u>	<u>Page</u>
Figure 1.1. Microenvironment in breast cancer.	1
Figure 1.2. Hypotheses: (1) Soluble EGF (2) Matrix-bound EGF (3) Cell-bound EGF. .	4
Figure 2.1. Cell-on-a-chip workflow.	7
Figure 2.2. 3D Hydrogel drop model.	9
Figure 3.1. BCC cells did not show chemotaxis towards macrophages whereas macrophages showed chemotaxis towards BCC.	12
Figure 3.2. Macrophages but not macrophage-derived-matrix modulated adhesion and motility of BCC in an EGF-dependent manner.	16
Figure 3.3. Cell shape changed as a function of the underlying substrate.	17
Figure 3.4. Cell motility changed as a function of the underlying substrate.	18
Figure 3.5. Live cell imaging on Matrigel.	19
Figure 3.6. Live cell imaging on Matrigel in the presence of iressa.	20
Figure 3.7. Live cell imaging on macrophage-derived-ECM.	21
Figure 3.8. Live cell imaging on macrophage-derived-ECM in the presence of iressa. .	22
Figure 3.9. Live cell imaging on disperse macrophage culture. Macrophages in red, MDA-MB-231 cells in green, labeled with CellTracker dyes.	23
Figure 3.10. Live cell imaging on disperse macrophage culture in the presence of iressa. Macrophages in red, MDA-MB-231 cells in green, labeled with CellTracker dyes.	24
Figure 3.11. Live cell imaging on bare glass surface.	25
Figure 3.12. Co-culture of BCC with macrophages in matrigel changed their multicellular organization.	27
Figure 3.13. Co-culture of BCC with macrophages in collagen changed their multicellular organization.	29
Figure 3.14. Macrophages reduced and promoted migration of BCC in matrigel and collagen, respectively.	31
Figure 3.15. Endocytosis of EGFR in suspended BCC.	32
Figure 3.16. Adherent BCC endocytosed EGFR when in contact with macrophages. .	33

LIST OF TABLES

<u>Table</u>	<u>Page</u>
Table 3.1. CSF-1 but not EGF was secreted.....	13
Table 3.2. Significances of the changes in the individual percentiles of L, B, M structures of BCC cultured in matrigel alone or in the presence of macrophages. *Two sample t-test between percents.	28
Table 3.3. Significances of the changes in the individual percentiles of R, A, P, C structures of BCC cultured in collagen alone or in the presence of macrophages. *Two sample t-test between percents.	30

CHAPTER 1

INTRODUCTION

Metastasis is the leading cause of death for cancer patients. Metastasis defines both the process of spreading of cancer cells from the primary tumor and the resulting secondary tumors. During metastasis of carcinoma (cancer of epithelial tissue), tumor cells degrade the underlying basement membrane and degrade into the connective tissue, migrate towards blood vessels, intravasate, extravasate and seed secondary sites in distant organs (Quail and Joyce 2013).

Stephen Paget's seed and soil hypothesis suggests that both the tumor cell and the microenvironment determine the sites where metastases occur (Paget 1989, Mendoza and Khanna 2009). The breast cancer microenvironment is composed of extracellular matrix (ECM), growth factors, chemicals and stromal cells such as macrophages, fibroblasts and endothelial cells (Liotta and Kohn 2001, Gupta and Massague 2006, Alphonso and Alahari 2009) (Figure 1.1).

Microenvironment in Breast Cancer	
<u>Cells</u>	<u>Extracellular matrix</u>
Cancer cells Normal epithelial cells	Collagens Laminin
Macrophages Fibroblasts	Fibronectin
Endothelial cells and others	Hyaluronan
	Nidogen/entactin
	Heparan sulfate proteoglycan and others
<u>Growth factors</u>	<u>Chemicals</u>
Epidermal growth factor Fibroblast growth factor	Reactive oxygen species
Vascular endothelial growth factor and others	Transforming growth factor
	Metal ions and others

Figure 1.1. Microenvironment in breast cancer.

The relationship between tumor cells, ECM and soluble growth factors has been studied more than the intercellular interactions. Studies of tumor cells and stromal cells have explored tumor cell – macrophage (Goswami et al. 2005), tumor cell – fibroblast (Studebaker et al. 2008) and tumor cell – endothelial cell interactions (Mierke et al. 2008). Most research to date has focused on the cancer cells rather than the microenvironment: 90% of the papers on cancer and microenvironment are published in the last ten years (Web of Science). Yet, microenvironment is an important target for therapeutic purposes (Hu and Polyak 2008): Bissell and colleagues succeeded in reverting the malignant phenotype of breast cancer cells to normal by blocking $\beta 1$ integrins (Weaver et al. 1997, Kenny and Bissell 2003). However, an in-depth and cohesive understanding of tumor cell interactions with the microenvironment is lacking.

As cancer cells metastasize, they interact with various extracellular molecules and stromal cells such as macrophages and fibroblasts (Condeelis and Pollard 2006, Marusyk et al. 2016). Macrophages have been shown to promote invasion and change multicellular organization of cancer cells (Pollard 2004, Ward et al. 2015). While interactions of tumor cells and macrophages have been perceived as a paracrine loop (Knutsdottir, Condeelis, and Palsson 2016, Wyckoff et al. 2004), an in-depth understanding of the mechanistic basis of this interaction is lacking.

Growth factors act as intercellular signaling molecules that promote various processes such as cell growth, adhesion and motility. Growth factors can be soluble, transmembrane or extracellular matrix bound proteins (Massague and Pandiella 1993, Taipale and KeskiOja 1997). Epidermal growth factor (EGF) is one of the seven ligands of EGF receptor (EGFR also known as ErbB1), and is the most studied member of the ErbB receptor family. While other EGFR ligands can bind to different members of the ErbB family, EGF binds only to EGFR (Carpenter and Cohen 1990, Harris, Chung, and Coffey 2003, Singh and Harris 2005). In addition, EGFR expression correlates with poor prognosis in breast cancer (Memon et al. 2006, Sainsbury et al. 1985).

The challenge of determining the physiologically relevant mechanism of action of EGF and its receptor is that *in vitro* set-ups do not reflect the *in vivo* microenvironment and that pertinent *in vivo* experiments are far too complicated. In standard cell culture, soluble EGF is provided through a micropipette to the growth medium and breast cancer cells show chemotaxis, i.e. move towards the source of EGF.

However, the experimental setting of culturing cells on a 2D surface with liquid medium on top, does not represent *in vivo* conditions. In the organism, cells are embedded in a 3D matrix. Some cells produce their own EGF while some depend on other cells as the EGF source. Mature EGF (6 kDa) is not detected in conditioned medium (Dickson et al. 1986, Vlaicu et al. 2013). It is also known that soluble EGF and conditioned medium of macrophages do not promote breast cancer cell invasion into collagen matrix and breast cancer cells do not invade into collagen if they are not co-cultured with macrophages (Goswami et al. 2005). Furthermore, it has been shown that EGFR can be activated with membrane bound ligands (Iwamoto, Handa, and Mekada 1999, Singh et al. 2004). Yet, EGF has both positively and negatively charged residues and charged molecules can bind the extracellular matrix (ECM) (Lieg, Baumgartel, and Bausch 2009). What is more, growth factors such as HB-EGF, FGF and VEGF have specific domains that can bind ECM molecules (Taipale and KeskiOja 1997). Furthermore, cells can move by holding on to surface immobilized molecules, which is defined as haptotaxis (Aznavoorian et al. 1990).

Based on the above, we tested the hypotheses that (1) Breast cancer cells show chemotaxis to EGF that diffuses in the ECM. (2) Breast cancer cells show haptotaxis to EGF that is bound to the ECM. (3) Breast cancer cells are stimulated by binding EGF that is on the cell surface of macrophages (Figure 1.2).

If EGF is soluble in a 3D matrix, breast cancer cells can move towards macrophages which are the source of EGF. Breast cancer cell motility will increase with proximity to macrophages (Figure 1.2 top). If EGF binds ECM, breast cancer cells will require to contact the parts of ECM with bound EGF to move (Figure 1.2 middle). In this case, EGF-specific antibodies will detect EGF in the ECM produced by macrophages; ECM produced by macrophages will stimulate breast cancer cell motility. If however, EGF stays on the surface of macrophages, breast cancer cells will not invade into matrix without direct contact to macrophages (Figure 1.2 bottom). In this case, EGF-specific antibodies will detect EGF on the surface of macrophages.

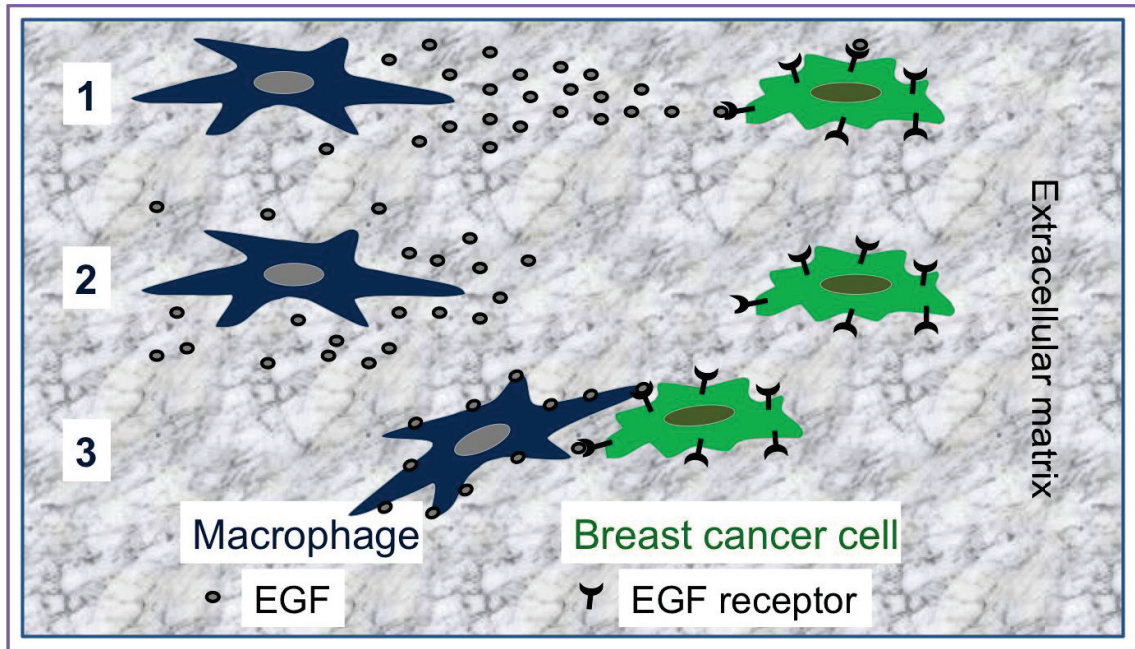


Figure 1.2. Hypotheses: (1) Soluble EGF (2) Matrix-bound EGF (3) Cell-bound EGF.

Breast cancer is the leading cancer type for women in Turkey as it is worldwide. However, we have not reached the desired diagnostics or therapy levels. Currently, success rate of clinical trials is only 10% (Woodcock and Woosley 2008). Almost all *in vitro* testing and even some animal models do not provide the orthotopic setting of the relevant cancer (McMillin et al. 2010). Thus better *in vitro* systems that can mimic the *in vivo* microenvironment are needed (Wolf et al. 2009). In addition, there is no ongoing research on the topic of 3D cancer microenvironments in Turkey.

Nanotechnology is providing powerful tools for life scientists. Lithography and other processes of micro-electro-mechanical systems used in the semiconductor industry are now being applied to cell and molecular biology to fabricate microarrays, protein chips and other lab-on-a-chip devices (They et al. 2005, Pesen and Haviland 2009, Chen et al. 1997, Cavalcanti-Adam et al. 2007). UV photolithography is a high throughput and versatile technique to create both 2D (surface) and 3D (microfluidic) patterns (Young and Simmons 2010, Qin, Xia, and Whitesides 2010). UV lithography enables us to fabricate portable devices with patterns scaling from micrometers to millimeters and liquid handling volumes of microliters.

Using UV lithography, we created 3D controlled microenvironments where breast cancer cells and macrophages were cultured at specific distances from each other.

This approach forms the foundation of an experimental system that allows us to investigate the interactions of breast cancer cells and various stromal cells. In addition, the experimental system has the potential to allow the study of many different cell types simultaneously. Such 3D controlled microenvironments facilitate and improve research on inter-cellular communication and allow us to develop new diagnostic and therapeutic lab-on-a-chip devices. The results achieved in this interdisciplinary thesis project, in terms of both technology and concept, will seed new projects.

Most widely used *in vitro* cell culture systems neither reflect the organization and complexity of the *in vivo* microenvironment nor provide extensive spatial and temporal control. On the other hand, microfluidics based cell-on-a-chip devices can provide both 2D and 3D settings, position multiple cell types at specific locations, provide static and dynamic chemical and physical inputs and gradients, and enable real time monitoring or visualization (Huh et al. 2010, Jeon et al. 2015, Keenan and Folch 2008, Au et al. 2016). Therefore, cell-on-a-chip devices are now proving to be a necessary step which links *in vitro* studies, *in vivo* animal models and clinical trials.

In this study, using a multidisciplinary approach including classical and up-to-date techniques such as cell-on-a-chip devices, we tested the three hypotheses outlined in Figure 1.2, with an emphasis placed on the 3rd hypothesis that a juxtacrine interaction is required for the activity of macrophage-derived-EGF on breast cancer cells.

CHAPTER 2

MATERIALS AND METHODS

2.1. Cell Culture

MDA-MB-231 (BCC) and RAW264.7 macrophages were acquired from ATCC (LGC Standards GmbH, Germany). BCC and macrophages were grown in tissue culture treated petri dishes in DMEM supplemented with 10% FBS, 1X penicillin-streptomycin, 1X L-glutamine and in non-treated petri dishes in RPMI supplemented with 5% FBS, 1X penicillin-streptomycin, 1X L-glutamine, respectively, at 37°C, 5% CO₂. BCC and macrophages were trypsinized and mechanically collected for sub-culturing, respectively.

2.2. Cell-on-a-chip Experiments

Fabrication of the cell-on-a-chip devices was performed as previously described (Ozdil et al. 2014) (APPENDIX A) and schematically summarized in Figure 2.1. Cell laden (6.5×10^6 cells/ml) and cell-free matrigel (354234, Corning) or collagen gels (354249, Corning) were loaded to the corresponding channels and polymerized at 37°C 5% CO₂ for 15 min. Then culture media were loaded into the medium reservoirs. The samples were kept at 37°C and 5% CO₂ for 7-14 days. Partially overlapping raster-scan phase-contrast images of fields of interest in cell-on-a-chip devices were acquired on at least days 1, 3 and 5 using an Olympus CX41 microscope or a Euromex OX.3120 microscope equipped with a Dino-Lite Eyepiece Camera and imaging software (DinoCapture 2.0). Images were stitched using Photoshop (Adobe).

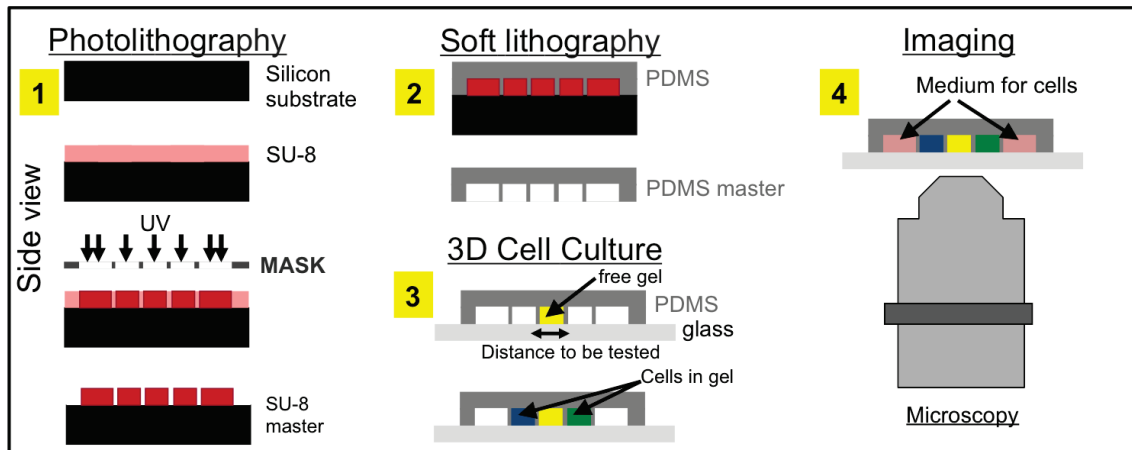


Figure 2.1. Cell-on-a-chip workflow.

For quantification of migration of co-cultured cells in cell-on-a-chip devices, each region between two PDMS posts was defined as an ROI and the maximum distance migrated in each ROI was measured using ImageJ.

2.3. Protein Quantification and ELISA

Macrophage-derived-matrix and cancer cell-derived-matrix were prepared by seeding 21K RAW 264.7 cells per cm^2 and 51K MDA-MB-231 cell per cm^2 and culturing cells for 7 days prior to sample collection. Macrophages and cancer cells were removed using 2M urea. Conditioned medium was prepared by culturing confluent cells for 24 hours in serum-free medium. Samples were collected and processed for Bradford (39222.02, Serva), EGF Mouse ELISA (ab100679, Abcam) and CSF Human ELISA (ab100590, Abcam) assays according to the manufacturers' instructions.

2.4. Live Cell Imaging

BCC were starved in serum free Leibowitz's medium supplemented with BSA, collected using cell dissociation buffer (Biological Industries, Israel) and re-suspended in starvation medium and added on glass, matrigel, macrophage-derived-matrix or macrophages. Imaging was started immediately using an Olympus IX70 microscope

equipped with a heating plate set to 37°C. Phase-contrast images were captured with a Euromex camera with the ImageFocus Software every 30 seconds.

For mgel surfaces, 100 µg/ml matrigel was used for coating glass coverslips. For MCm surfaces, macrophage derived matrix was prepared by seeding 48K RAW 264.7 cells per 15mmx15mm area of a glass coverslip and culturing cells for 7 days prior to the live cell imaging experiment. Macrophages were removed using 2M urea. For MC surfaces, 6K cells were seeded, cultured for 7 days and used after rinsing with serum-free medium.

For live cell experiments on MC surfaces, BCC and macrophages were stained with CellTracker Green CMFDA or Blue CMAC (Molecular Probes), respectively, according to the manufacturer's instructions. Fluorescence images were captured for the first and last time points.

BCC were treated with 2 µM Iressa ('Gefitinib' sc-202166, Santa Cruz Biotechnology) for 16 hours prior to using the cells in live cell imaging experiments. Medium with Iressa was replenished just before live cell imaging.

Cell area, circularity and aspect ratio of the cells were measured from manually tracked cell boundaries using ImageJ. BCC cells were classified as 'round' or 'spread' on different surfaces. If a cell had any flat protrusions, it was classified as spread.

For motility, cell nuclei were manually tracked over time. Speed was calculated as the ratio of the net distance travelled to time for each time interval of 15 minutes. Persistence was calculated as the ratio of the net distance to the total distance.

2.5. 3D Co-culture Hydrogel Experiments

2×10^6 cells/ml of BCC and macrophages were seeded alone or together in 1:1 matrigel or 2 mg/ml collagen hydrogel drops of 2 µl in multi-well plates which were placed upside down during hydrogel polymerization. Another 15 µl of the corresponding cell-free hydrogel was then polymerized on the cell-laden hydrogels. Next, macrophage culture medium was added to the wells, and cells were cultured at 37°C and 5% CO₂. Image acquisition was performed as for cell-on-a-chip experiments.

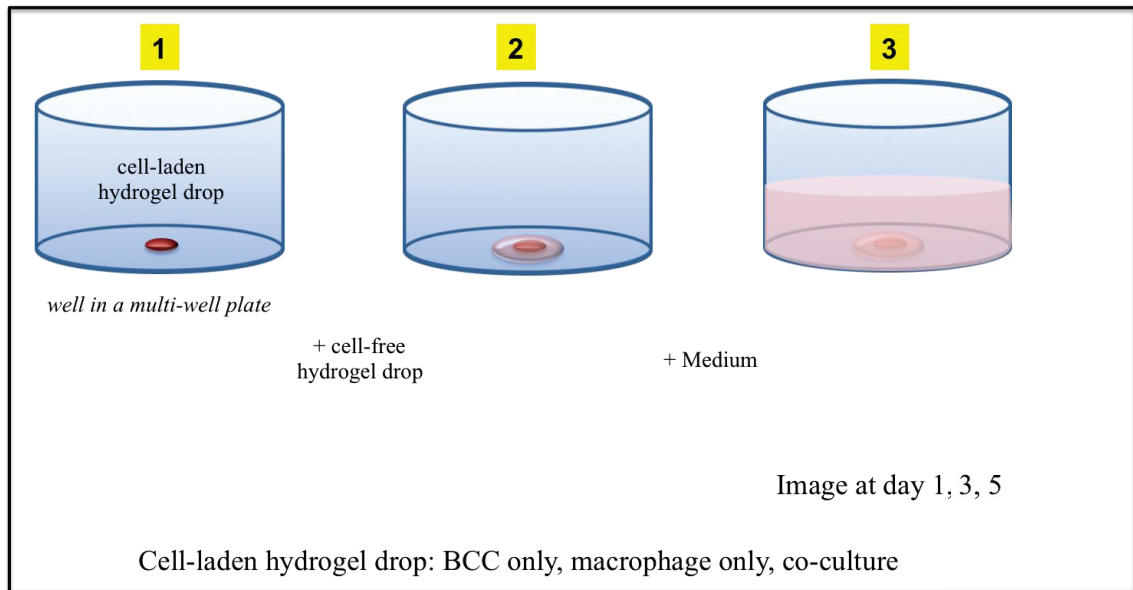


Figure 2.2. 3D Hydrogel drop model.

The outermost 328 μm (250 pixels) ring of the cell-laden matrigel drops was examined. A line structure was defined to contain at least 2 cells and be more than 100 pixels in length. A branch was defined to contain at least 3 cells and to have a ‘Y’ or ‘T’ shape. A multicellular complex was defined to contain at least 4 cells which had connections with each other.

The boundary at the cell-laden and cell-free collagen was examined. An along cell was defined to be aligned along the boundary. A perpendicular cell was defined to be perpendicular to the boundary. Round and clustered cells at the boundary were also counted.

Assignments of different structures were performed by two or three independent observers and cross-checked.

2.6. Endocytosis in Suspended Cells

BCC were starved and incubated in a cell dissociation buffer (Biological Industries, Israel) for collection. BCC were then treated with 3.5 nM EGF or macrophages in suspension for 10 minutes. Samples were then fixed with 4% paraformaldehyde and processed for immunostaining with EGFR (D38B1) XP rabbit mAb (4267, Cell Signaling Technology, 1:100), anti-rabbit secondary antibody Alexa

Fluor 555 Conjugate (4413, Cell Signaling Technology, 1:200) and Alexa Fluor 488 Phalloidin (8878, Cell Signaling Technology, 1:200). Fluorescence images were captured with an Olympus IX83 microscope equipped with a DP73 camera and cellSens software. Fluorescence signal of EGFR localized to the membrane divided by the total cellular signal was measured using ImageJ.

2.7. Endocytosis in Adherent Cells

BCC were transiently transfected with EGFR-GFP, a gift from Alexander Sorkin (Addgene plasmid # 32751). BCC were starved and treated with 3.5 nM EGF or suspended macrophages labelled with Blue CMAC (Molecular Probes). Images were acquired with a Zeiss Observer microscope equipped with an incubation chamber set to 37°C, an MRm camera and Zen software. BCC showing inward movement of EGFR-GFP from the cell membrane to the cytosol were counted as endocytosis positive.

2.8. Image Analysis

Photoshop (Adobe) and ImageJ (NIH) were used for image processing and analysis.

2.9. Statistical Analysis and Data Presentation

Mann-Whitney two-tailed test (MATLAB), χ^2 test (Microsoft Excel) and two sample t-test between percents (StatPac) were used to determine significances. Statistical significance was taken as $p < 0.05$. Data are represented as means \pm s.e.m. Detailed statistics and source data are available in Supplementary Dataset (APPENDIX C).

CHAPTER 3

RESULTS AND DISCUSSION

3.1. BCC cells did not show chemotaxis towards macrophages whereas macrophages showed chemotaxis towards BCC

To determine the mechanism of interaction between macrophages and BCC on the EGF – CSF-1 axis, in particular to determine how macrophage-derived-EGF acts on BCC, we first investigated chemotaxis in 3D cell culture (Figure 3.1). We used custom cell-on-a-chip devices comprising three neighboring hydrogel channels where constituents from adjacent channels had access to each other through gaps between regularly spaced posts that formed the borders between channels. We loaded cell-free matrix into the middle channel and then different cell-laden matrices into the left and right channels. The two reservoirs, each adjacent to the left and right channels, were filled with culture medium. Such a cell-on-a-chip design allowed assessment of the chemotactic responses between two cell types in a 3D cell culture setting. We initially used a cell-on-a-chip device where the two cell types embedded in matrigel were positioned at an equal distance of 2 mm from each other and the cell culture medium in the reservoirs was serum-free. Here, macrophages showed low level of migration towards BCC which, on the other hand, did not migrate. To remove any limitations due to the absence of serum and long distances between cells, we used another cell-on-a-chip design where the distance between the two cell types changed from 3 mm to 0.3 mm and the cell culture medium in the reservoirs contained serum (Ozdil et al. 2014). Here, macrophages showed prominent migration towards BCC which still did not migrate notably. These results showed that BCC did not show chemotaxis towards macrophages whereas macrophages did so.

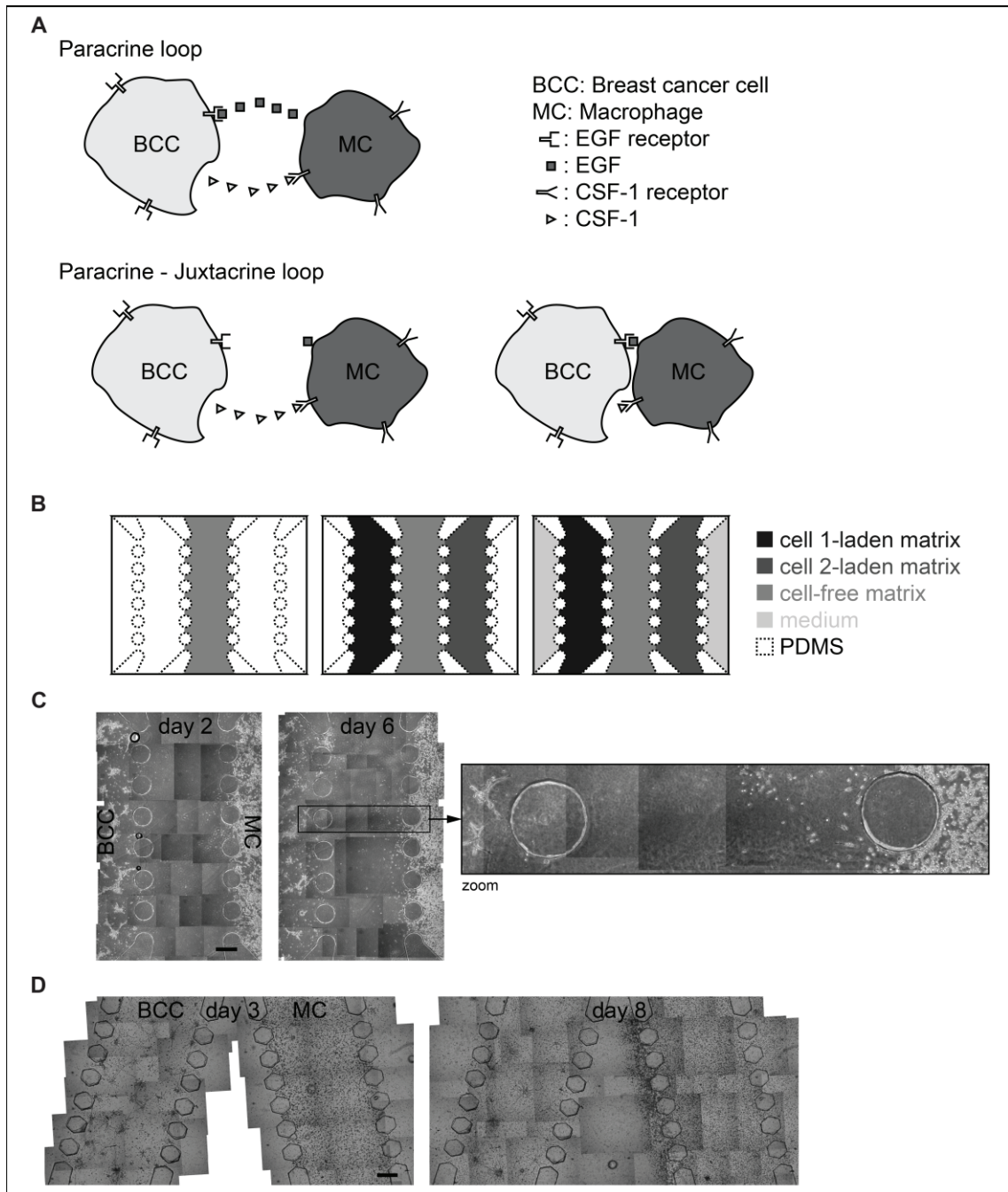


Figure 3.1. BCC cells did not show chemotaxis towards macrophages whereas macrophages showed chemotaxis towards BCC.

(A) Current and proposed model for interaction of BCC with macrophages. In the current model (top), BCC show chemotaxis towards macrophage-derived-EGF and macrophages show chemotaxis towards BCC-derived-CSF-1. In the proposed model (bottom), macrophage-derived-EGF is associated with macrophages and direct contact is required for interaction of macrophage-derived-EGF and EGFR on BCC. (B) Cell-on-a-chip design to test distant interactions. Cell-free matrix was loaded into the middle channel. Cell-laden matrices were loaded into channels on either side of the middle channel. The two reservoirs neighbouring the cell-laden channels were filled with cell culture medium. (C) Representative image for a cell-on-a-chip device where the cell-free middle channel had a constant width (from 2 cell-on-a-chip devices). (D) Representative image for a cell-on-a-chip device where the cell-free middle channel had a varying width (from 3 cell-on-a-chip devices). (Scale bars, 500 μm .)

3.1.1. ELISA Results

To confirm that BCC provided a soluble signal whereas macrophages did not, we determined the EGF and CSF-1 content of macrophage- and BCC-conditioned medium, macrophage- and BCC-derived-extracellular matrix (ECM) and the cells themselves using ELISA. The majority of the protein and the growth factors were present in cells, as expected (Table 3.1). The ECMs from MC and BCC constituted about 37% and 19% of the total protein and they contained 7% and 12% of EGF and CSF-1, respectively. The conditioned medium of macrophages was 1% of the total protein content and it contained only 1% of the total EGF, showing that EGF was not secreted. Yet, the conditioned medium of BCC was almost 1% of the total protein content and contained 35% of the total CSF-1 showing that CSF-1 was secreted. Together, cell-on-a-chip and ELISA results indicated that macrophages could show chemotaxis to BCC-derived-CSF-1 whereas BCC did not show chemotaxis to macrophages in consistent with the lack of EGF in macrophage-conditioned-medium.

		Cells	Matrix	CM	Total*
Macrophages	EGF %	92	7	1	100
	Total Protein %	62	37	1	100
BCC	CSF-1 %	53	12	35	100
	Total Protein %	81	19	1	100

Table 3.1. CSF-1 but not EGF was secreted.

ELISA and total protein analysis for BCC, BCC-derived matrix, BCC-conditioned medium, MC, MC-derived matrix and MC-conditioned medium. *Total % can exceed 100 due to rounding.

3.2. Macrophages but not macrophage-derived-matrix modulated adhesion and motility of BCC in an EGF-dependent manner

Since growth factors may bind ECM, we investigated adhesion and motility of BCC on macrophage-derived-ECM (Figure 3.2, Figure 3.3 and Figure 3.4). BCC were imaged live as they were introduced onto glass coated with matrigel (mgel), glass coated with macrophage-derived-ECM (MCm), glass dispersedly coated with macrophages (MC) and bare glass surfaces. During the first fifty minutes, BCC on mgel surfaces attached and spread, increasing their cell area 4.79 fold ($p < 0.0001$). Yet, BCC on the other surfaces did not spread significantly except on glass surface where there was a small (1.075 fold) increase in cell area ($p < 0.05$). At fifty minutes, cell area on mgel surfaces was larger than those on all other surfaces ($p < 0.005$). Circularity of BCC decreased in time on mgel ($p < 0.001$), but not on other surfaces. At fifty minutes, circularity of BCC on mgel surfaces was smaller than those on all other surfaces ($p < 0.001$). Aspect ratio of BCC did not change in time or between different surfaces. These results showed that presence of macrophages or macrophage-derived-ECM did not support initial cell attachment as well as matrigel. We also analyzed cell morphology at the end of 5 hours on each of the above mentioned surfaces in the presence and absence of iressa (gefitinib), an EGFR inhibitor (Wakeling et al. 2002). Areas of BCC decreased from mgel ($784.5 \pm 30.9 \mu\text{m}^2$) to MCm ($704.1 \pm 58.9 \mu\text{m}^2$) to MC ($383.5 \pm 32.3 \mu\text{m}^2$) to glass ($245.1 \pm 6.6 \mu\text{m}^2$) surfaces ($p < 0.036$). Although the addition of iressa did not change the cell area of BCC on MCm and glass surfaces, it decreased and increased cell area on mgel (0.74 fold) and MC (1.24 fold) surfaces, respectively ($p < 0.0001$). Circularity of BCC increased from mgel to MCm to MC to glass ($p < 0.0001$). Presence of iressa increased the circularity of BCC on mgel and glass surfaces whereas it decreased that on MC ($p < 0.0001$) surfaces. Aspect ratio of BCC was similar between mgel and MCm and decreased from MCm to MC to glass surfaces ($p < 0.0001$). Presence of iressa decreased and increased aspect ratio of BCC on mgel and MC surfaces, respectively ($p < 0.016$). These results showed that the presence of macrophage-derived-ECM supported adhesion and spreading of BCC as well as matrigel and better than the presence of macrophages. Presence of iressa affected adhesion on mgel and MC but not MCm surfaces suggesting that EGF was present in matrigel and was associated with macrophages.

We examined BCC motility on mgel, MCm and MC surfaces in the presence or absence of iressa during the first 5 hours of being introduced onto the surfaces of interest (Figure 3.2G-H, and Figure 3.4). Average speed of BCC on mgel (0.48 ± 0.06 $\mu\text{m}/\text{min}$) surfaces was larger than those on MCm (0.18 ± 0.02 $\mu\text{m}/\text{min}$) and MC (0.09 ± 0.01 $\mu\text{m}/\text{min}$) surfaces ($p < 0.00002$). Iressa did not have an effect on BCC on mgel and MCm surfaces probably because while the rich composition of matrigel allowed compensation, motility on MCm was minimal to begin with. Thus MCm surfaces promoted cell adhesion but not motility. Yet, presence of iressa increased the average speed of BCC on MC surfaces 2.5 fold ($p < 0.00001$), which was consistent with the increase in cell adhesion in the presence of iressa on MC surfaces because cells can be motile after they have adhered well enough and there is a positive feedback from adhesion to motility. Persistence of BCC on all surfaces was similar. Thus any EGF mediated effect on cell motility was apparent only on MC surfaces. These results aligned with ELISA results showing majority of EGF was associated with macrophages and cell adhesion data suggesting that macrophage-derived-EGF provided pro-motility input. Together, cell adhesion and motility results showed that BCC changed EGF-mediated-behavior on macrophages but not on macrophage-derived-ECM.

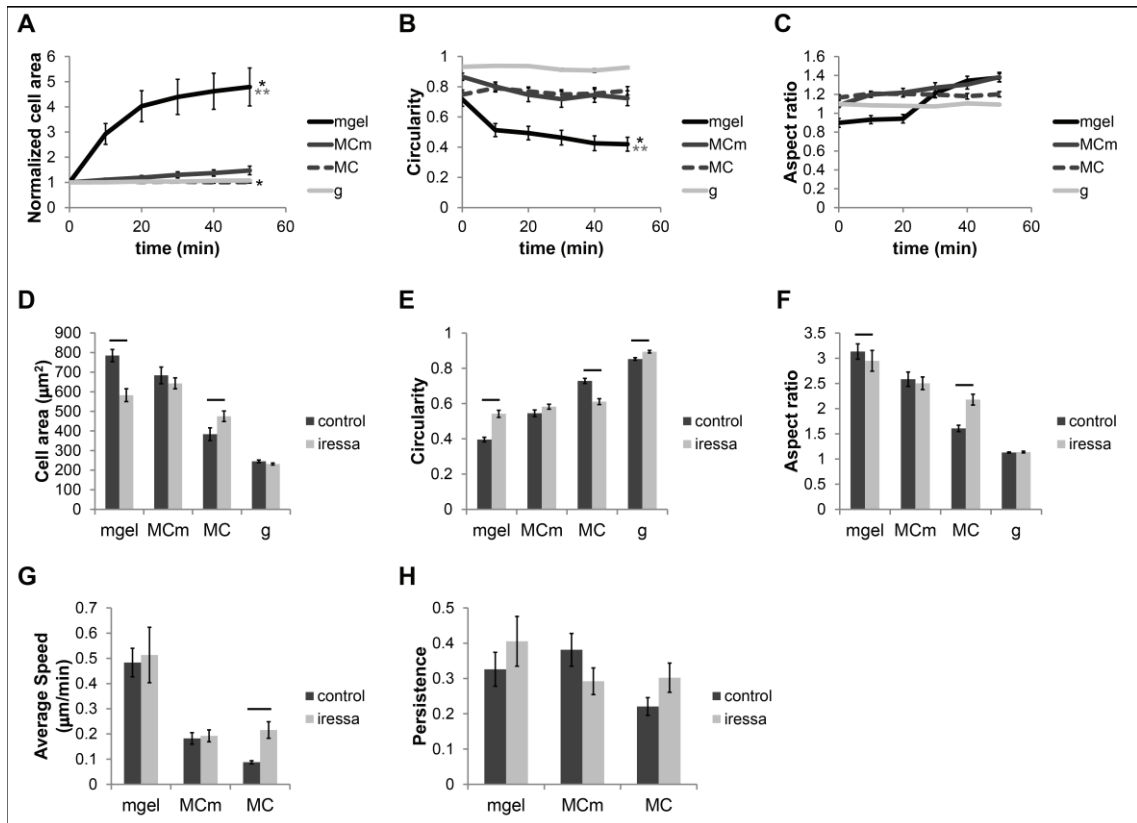


Figure 3.2. Macrophages but not macrophage-derived-matrix modulated adhesion and motility of BCC in an EGF-dependent manner.

Quantification of (A) area, (B) circularity and (C) aspect ratio of cells during the first 50 minutes of adhesion (mean \pm s.e.m. $n = 18, 24, 23, 6$ cells). Quantification of (D) area, (E) circularity and (F) aspect ratio of cells at 6 hours of adhesion in the presence and absence of iressa (mean \pm s.e.m. $n = 283, 145, 213, 97, 185, 255, 182, 130$ cells). Quantification of (G) average speed and (H) persistence of cells in the presence and absence of iressa (mean \pm s.e.m. $n = 20, 22, 29, 15, 24, 23$ cells). Asterisks show significant differences between $t = 0$ and 50 minutes. Double asterisks show significant differences between matrigel and all other three surfaces. Horizontal bars show significant differences between control and iressa groups.

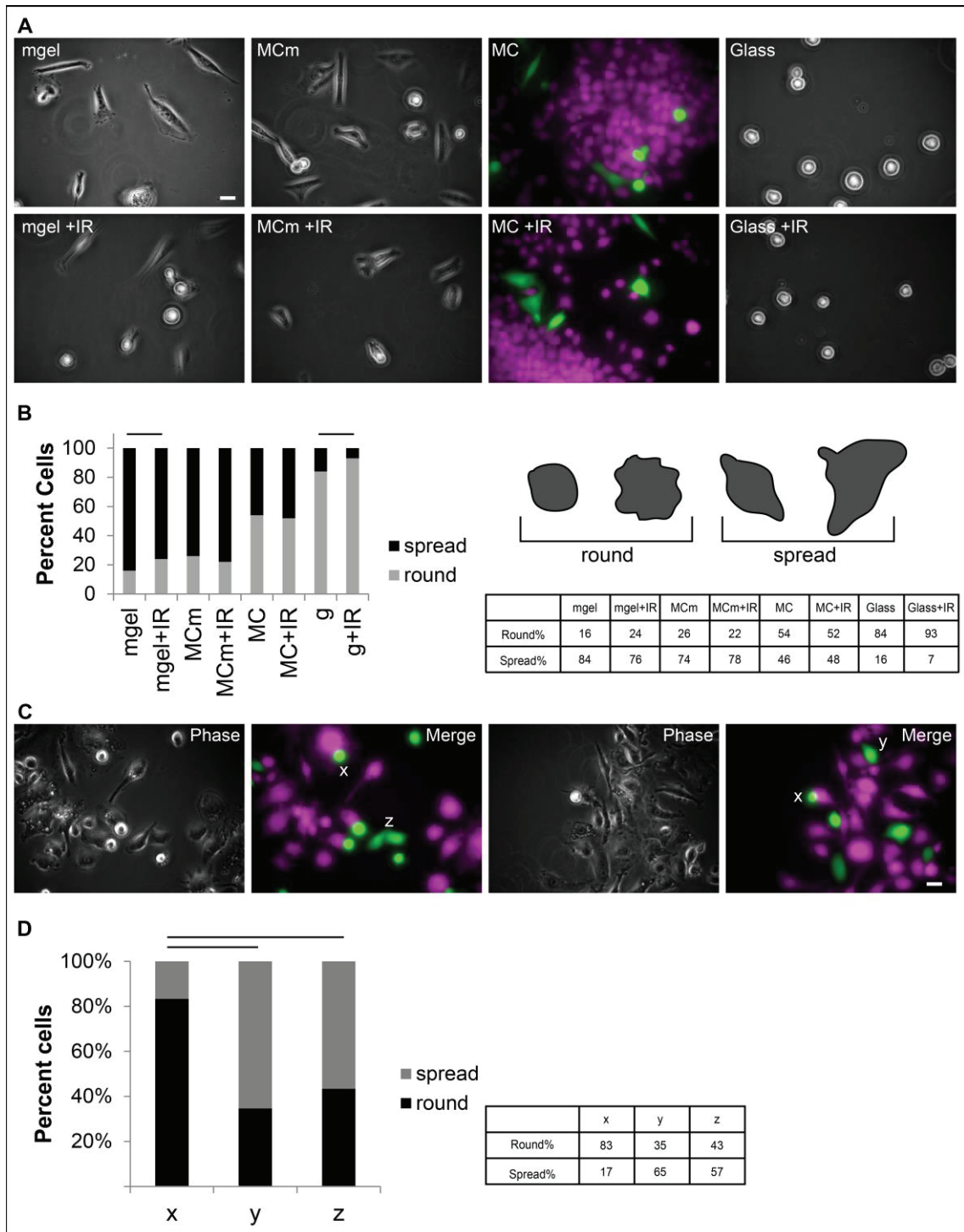


Figure 3.3. Cell shape changed as a function of the underlying substrate.

EGF dependency was observed for mgel and MC surfaces. (A) Representative images for BCC at 6 hours of adhesion on mgel, MCm, MC and glass surfaces in the presence and absence of iressa. Macrophages (magenta) were cultured for 7 days prior to addition of BCC (green). (Scale bars, 20 μm .) (B) Percentage of round and spread BCC cells at 6 hours of adhesion on mgel, MCm, MC and glass surfaces in the presence and absence of iressa (χ^2 test for $n = 280, 445, 273, 281, 545, 512, 359, 271$ cells). (C) Representative images for BCC on MC surface at 6 hours of adhesion. x: BCC on MC, y: BC in contact with MC, z: on MC-free area in the merged image of BCC (green) and MC (magenta) (χ^2 test for $n = 30, 75, 53$ cells). (Scale bars, 20 μm .) (D) Percentage of round and spread BCC cells on MC at 6 hours of adhesion (χ^2 test for $n = 30, 75, 53$ cells). Horizontal bars show significant differences.

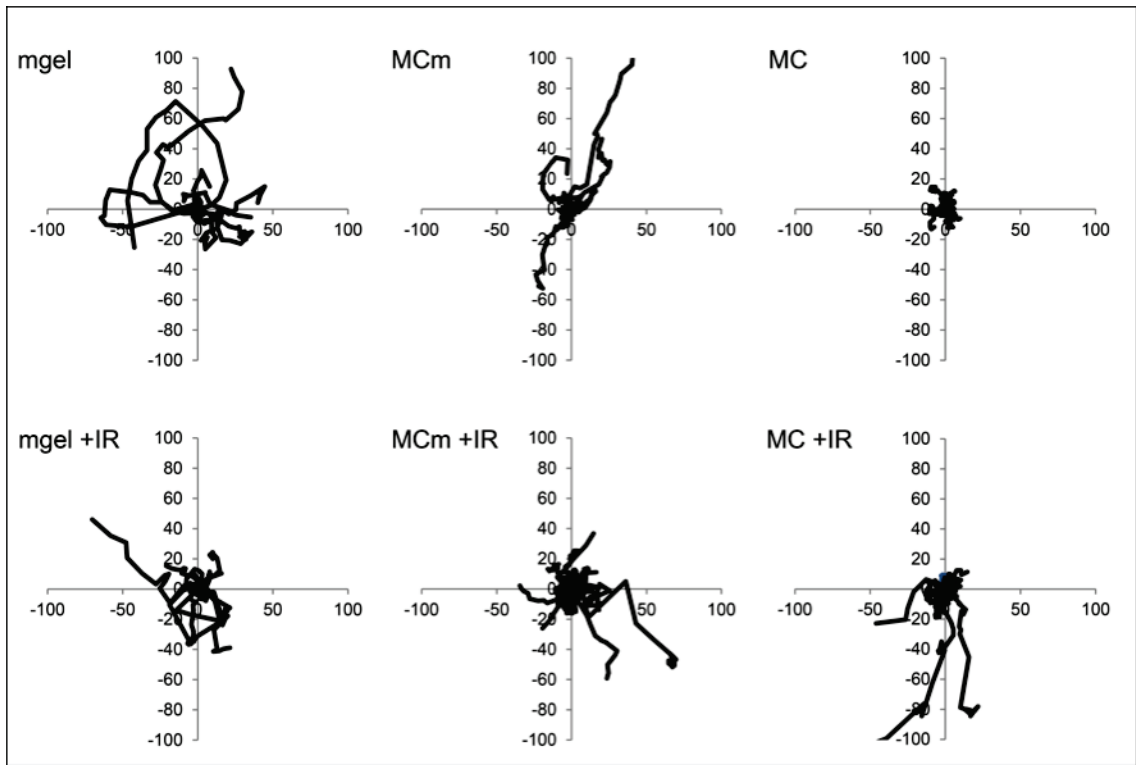


Figure 3.4. Cell motility changed as a function of the underlying substrate.

Cell tracks of BCC motility on mgel, MCm, MC and glass surfaces in the presence and absence of iressa during 5 hours of live cell imaging (for $n = 15-29$ cells).

3.2.1. Snapshots from 5 hours Long Live Cell Imaging at every 15 min

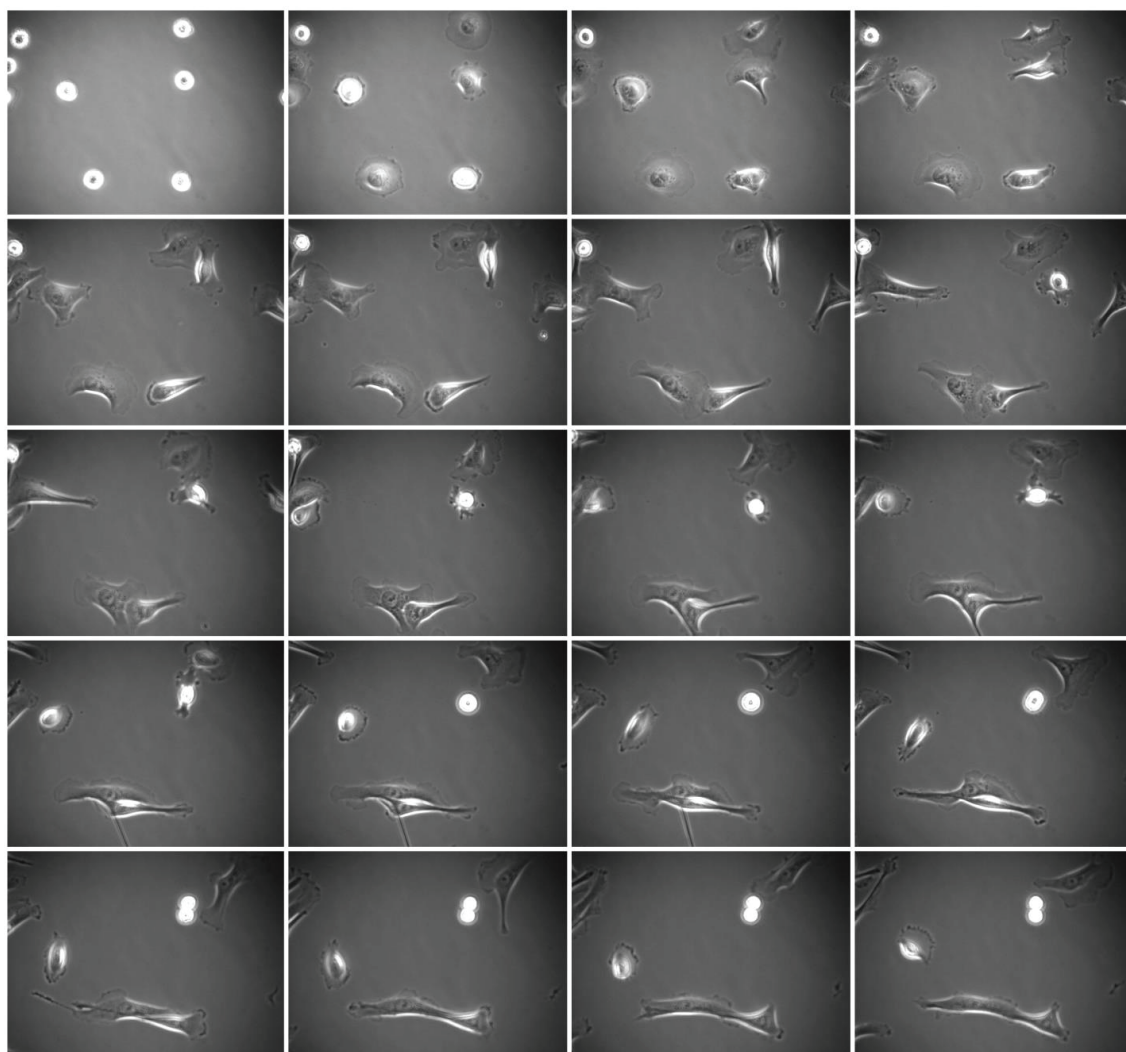


Figure 3.5. Live cell imaging on Matrigel.

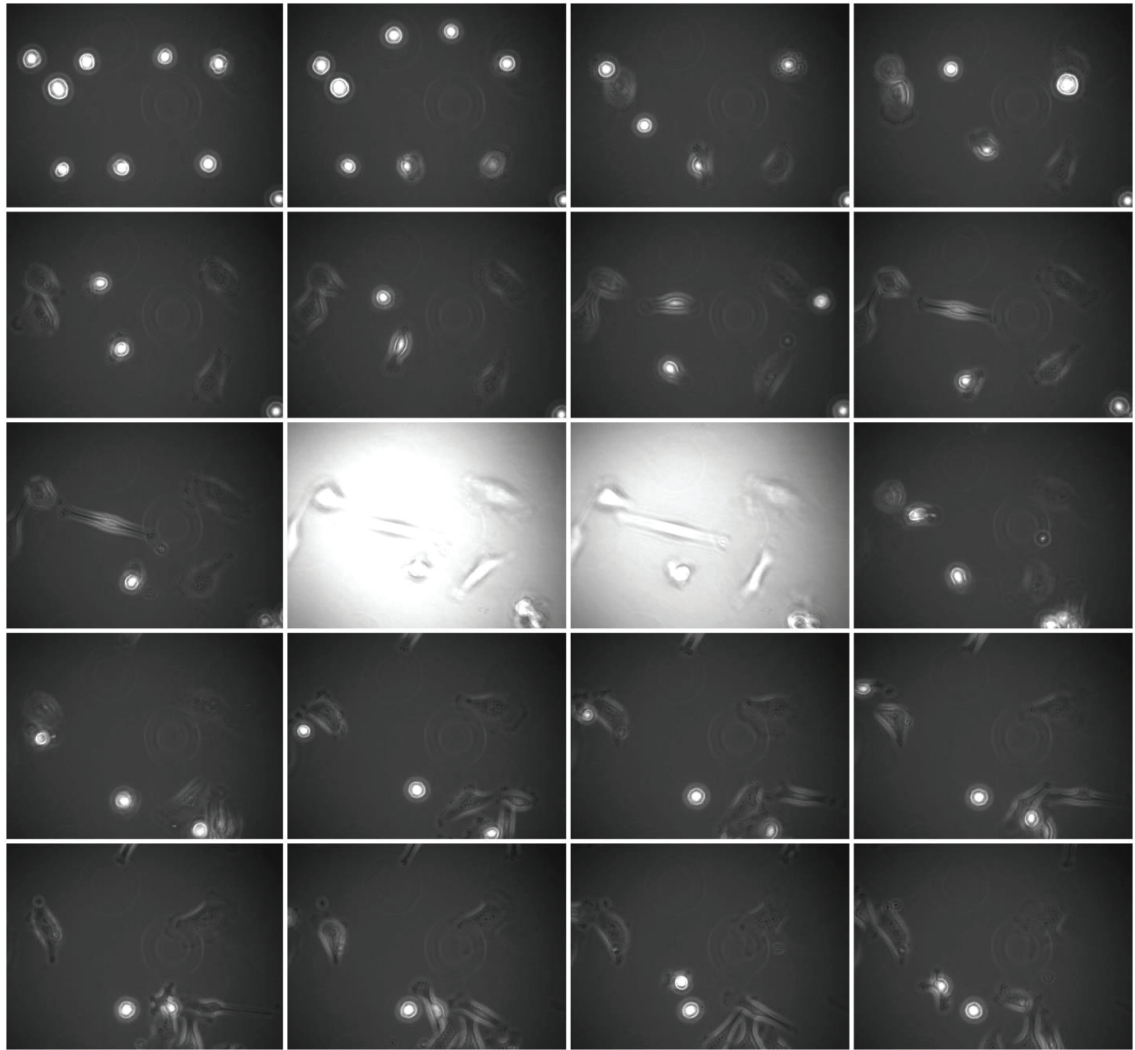


Figure 3.6. Live cell imaging on Matrigel in the presence of iressa.

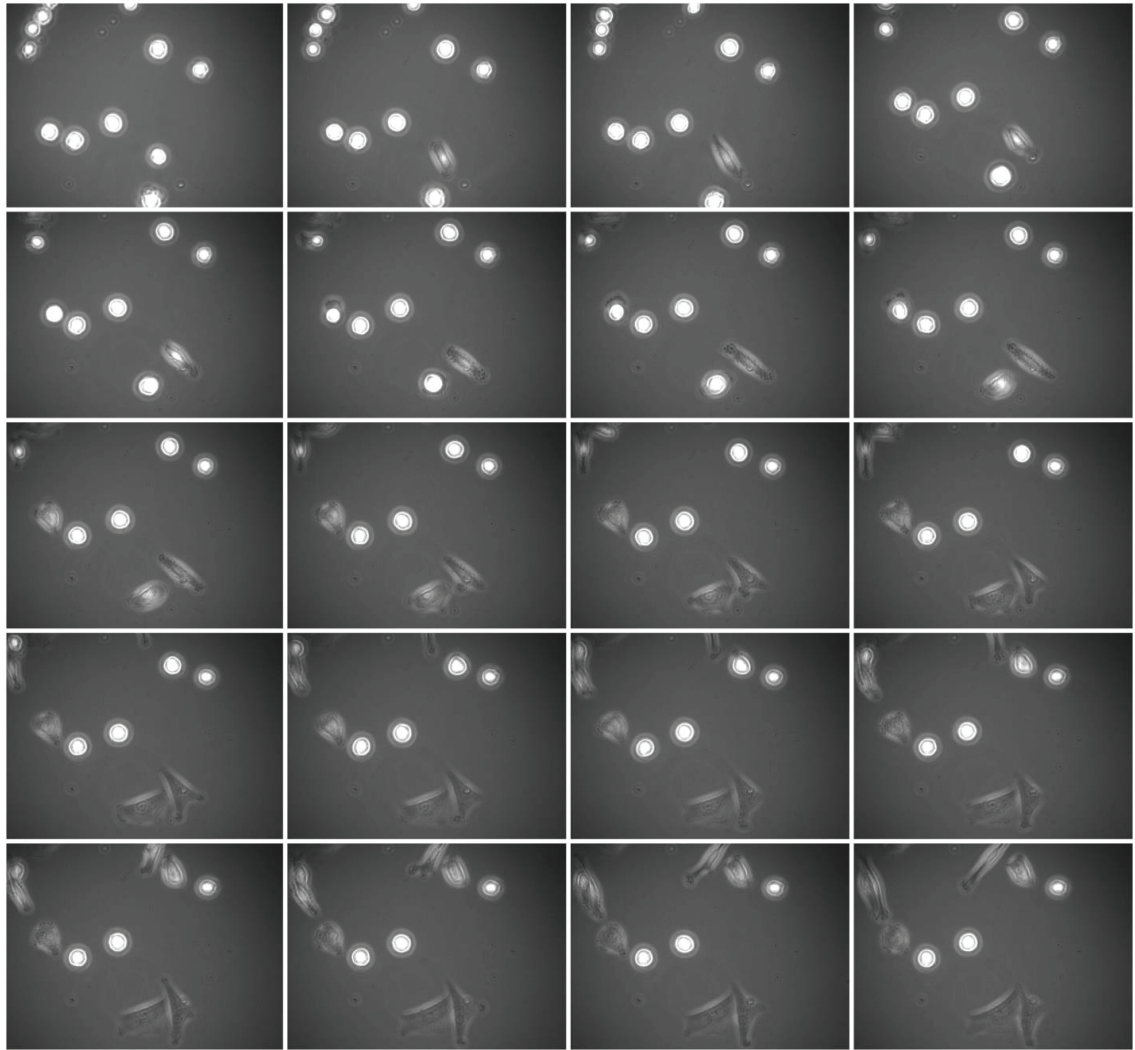


Figure 3.7. Live cell imaging on macrophage-derived-ECM.

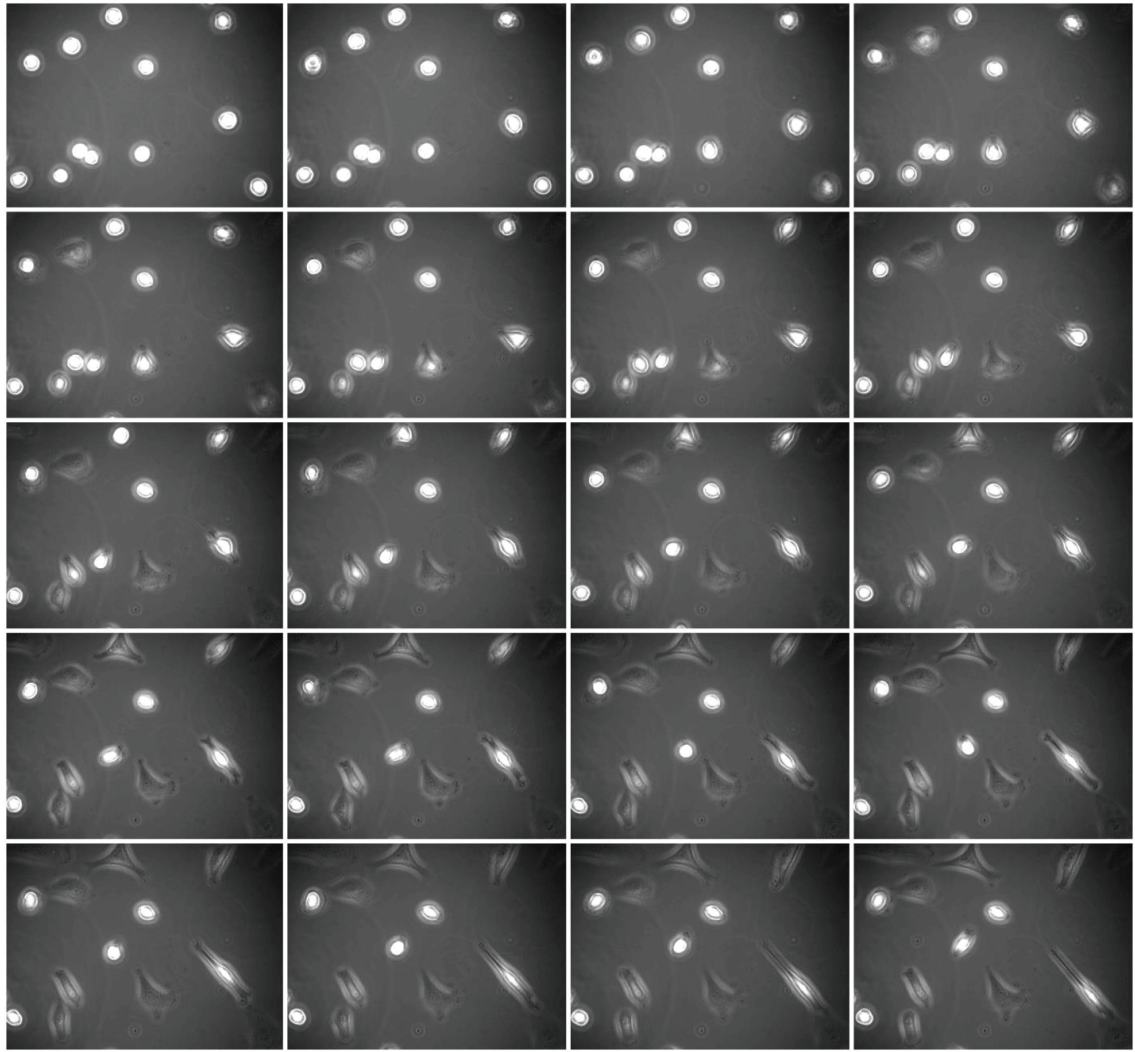


Figure 3.8. Live cell imaging on macrophage-derived-ECM in the presence of iressa.

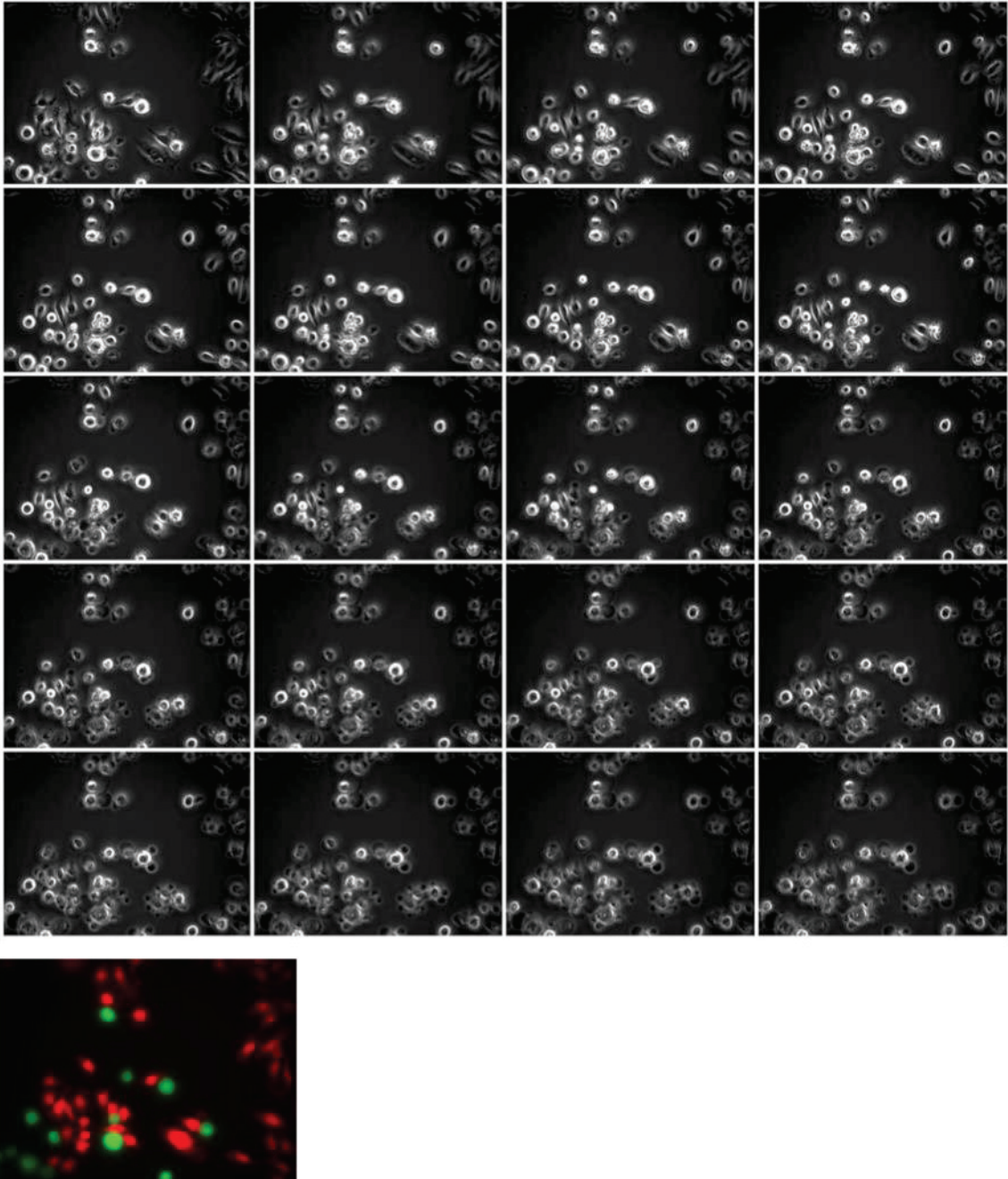


Figure 3.9. Live cell imaging on disperse macrophage culture. Macrophages in red, MDA-MB-231 cells in green, labeled with CellTracker dyes.

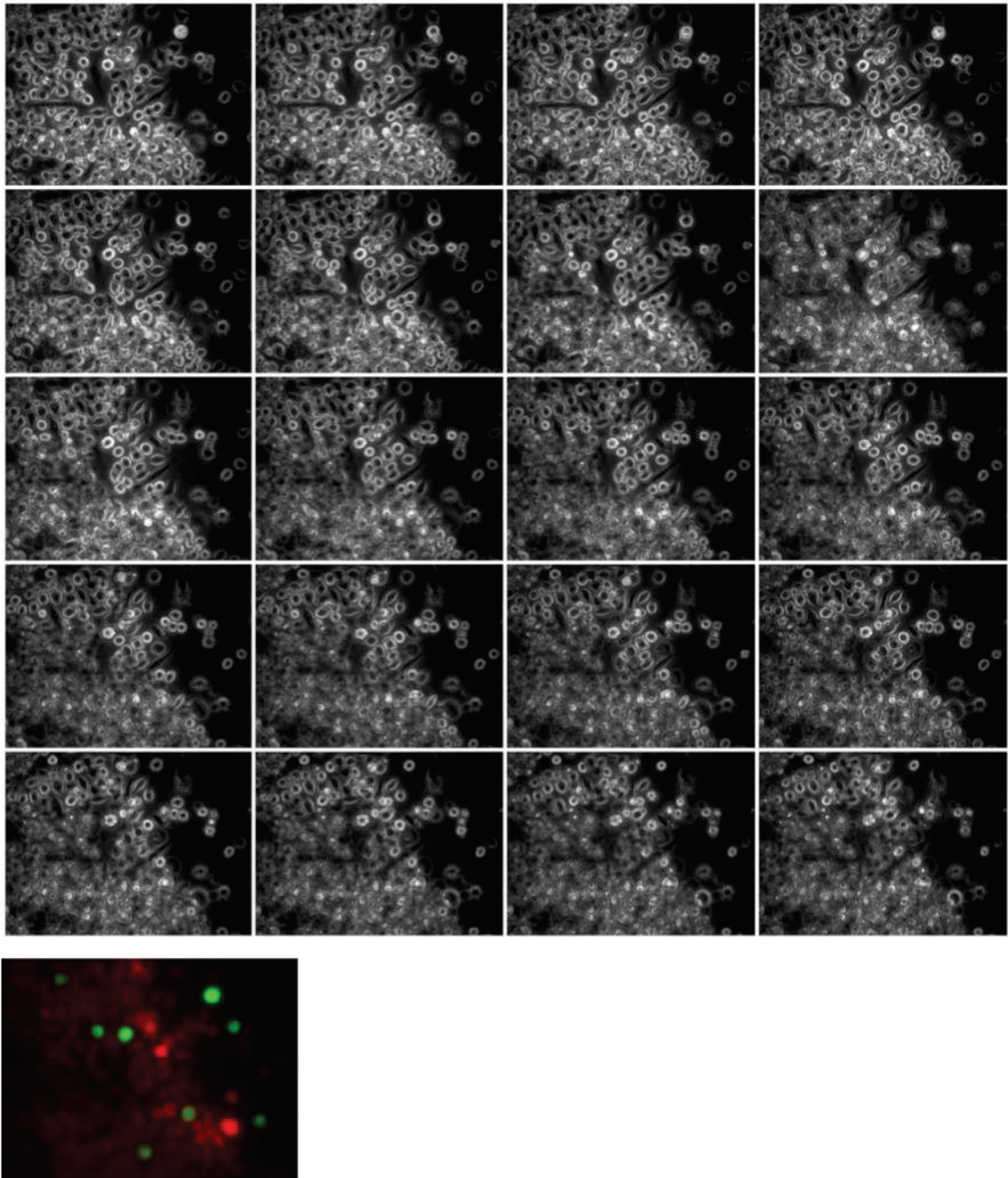


Figure 3.10. Live cell imaging on disperse macrophage culture in the presence of iressa. Macrophages in red, MDA-MB-231 cells in green, labeled with CellTracker dyes.

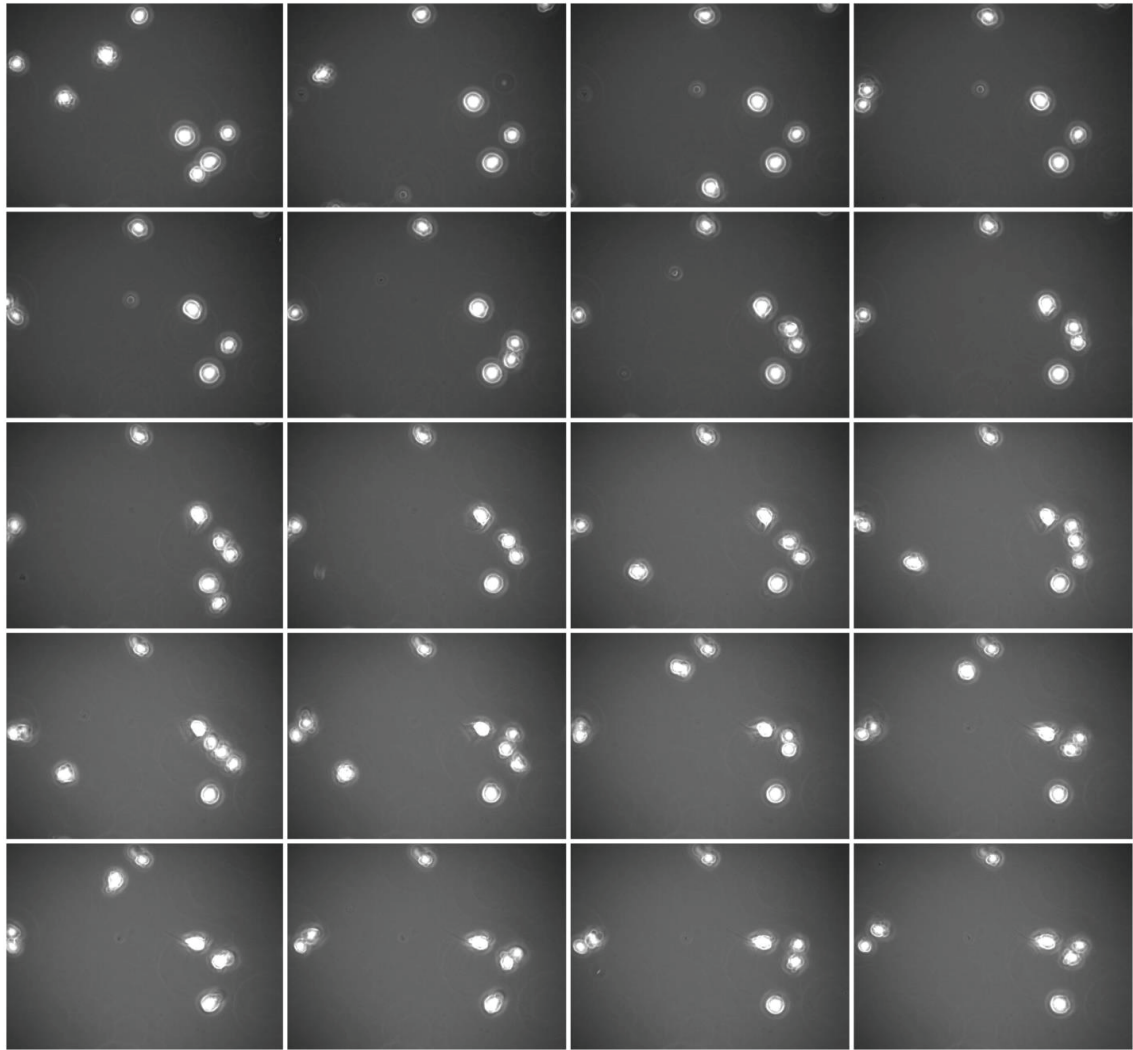


Figure 3.11. Live cell imaging on bare glass surface.

3.3. Co-culture of BCC with Macrophages in Hydrogel Drops or in Cell-on-a-chips

3.3.1. Co-culture of BCC with macrophages in matrigel or collagen hydrogel drops changed their multicellular organization

As cells can also interact with membrane-bound growth factors, it is possible that BCC interact with EGF which is macrophage-bound. In this case, direct contact with macrophages is likely to modulate phenotypes of BCC. Results for adhesion and

motility of BCC on MC surfaces reported above supported such a juxtacrine mode of interaction. Here, we further investigated BCC and macrophages in 3D co-culture (Figure 3.12 and Figure 3.13). The multicellular organization of BCC changed in matrigel and collagen hydrogel drops in the presence of macrophages. In matrigel, BCC alone organized into star-like multicellular complexes, branched structures or lines of cells. On day 5 of co-culture, presence of macrophages changed the percentile distribution of these structures (χ^2 $p < 0.002$). Percentage of branch and line structures decreased and increased, respectively (Percent t-test < 0.05) (Table 3.2). The number of branched structures decreased 3-fold per hydrogel drop ($p < 0.029$). In collagen, BCC appeared as round or elongated and along or elongated and perpendicular cells as well as clusters along the cell-laden hydrogel drop border. On day 5 of co-culture, presence of macrophages changed the percentile distribution of these structures (χ^2 $p < 5.77303E-14$). Percentage of along and clustered cells decreased and increased, respectively (Percent t-test < 0.05) (Table 3.3). The number of round cells and clusters per hydrogel drop decreased (1.9-fold) and increased (24-fold), respectively ($p < 0.041$). Thus 3D co-culture results showed that BCC and macrophages did interact, resulting in changes in single and multi-cellular organization in 3D.

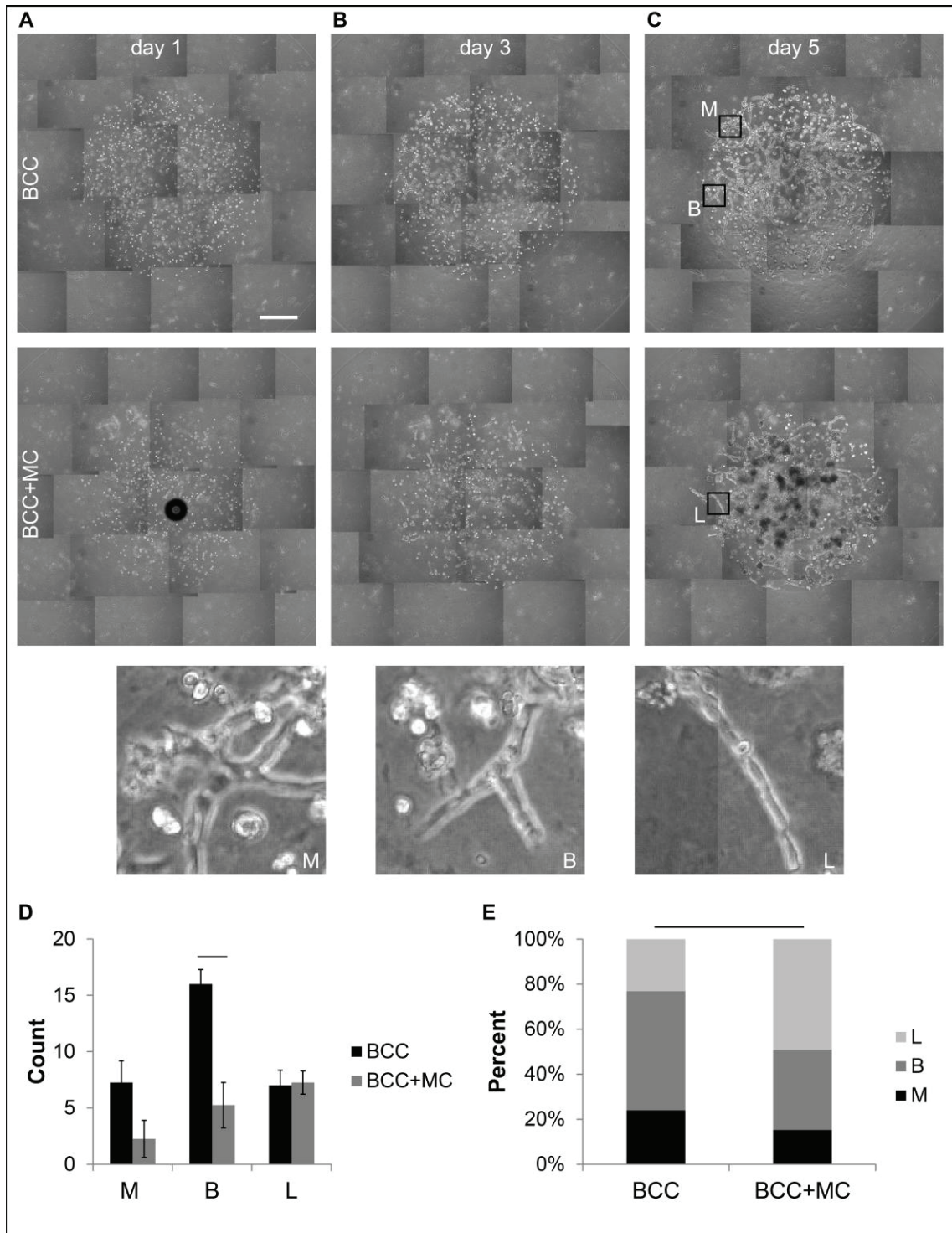


Figure 3.12. Co-culture of BCC with macrophages in matrigel changed their multicellular organization.

Presence of macrophages decreased the number of branched structures of BCC per hydrogel drop 3-fold ($p < 0.029$) and changed the percentile distribution of structures (χ^2 test $p < 0.002$). The multicellular organization of BCC in matrigel hydrogel drops alone or with the presence of macrophages on day1 (A), day 3 (B) and day5 (C). (Scale bars, 500 μm .) M: star-like multicellular complexes, B: branched structures, L: lines of cells. (D) The number of the M, B, L structures for BCC alone and BCC co-culture with MCC on day 5 (mean \pm s.e.m. $n = 121$, 59 structures). (E) The percentile distribution of the structures (χ^2 test). Horizontal bars show significant differences.

	BCC	BCC+MC	Significance*
L%	23	49	p<0.05
B%	53	36	p<0.05
M%	24	15	p>0.05

Table 3.2. Significances of the changes in the individual percentiles of L, B, M structures of BCC cultured in matrigel alone or in the presence of macrophages. *Two sample t-test between percents.

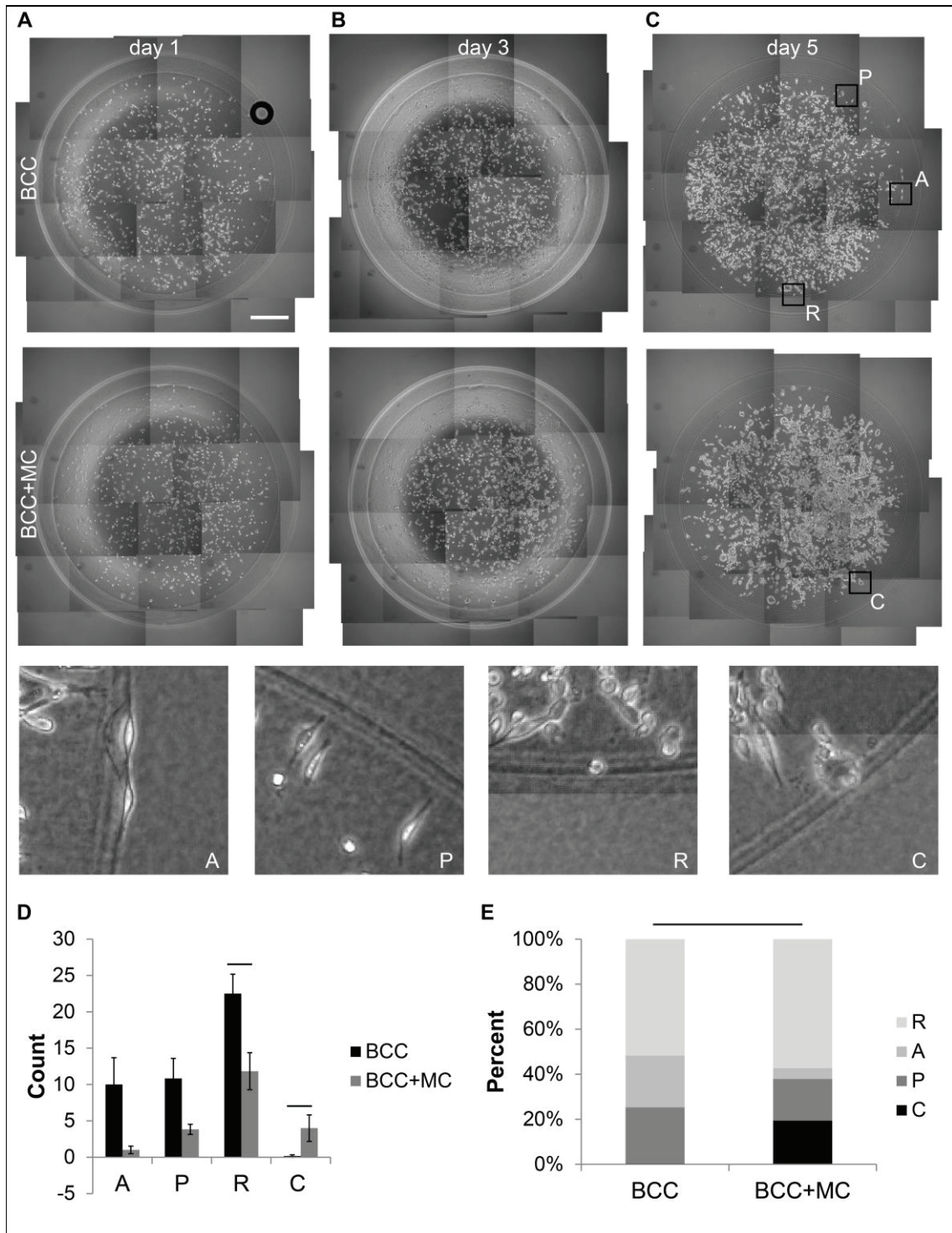


Figure 3.13. Co-culture of BCC with macrophages in collagen changed their multicellular organization.

Presence of macrophages decreased the number of round cells ($p < 0.015$) and increased the number of clusters per hydrogel drop ($p < 0.041$), respectively and changed the percentile distribution of structures (χ^2 test $p < 5.77E-14$). The organization of BCC alone or with the presence of macrophages in collagen hydrogel drops on day 1 (A), day 3 (B) and day 5 (C). (Scale bars, 500 μm .) A: elongated and along, P: elongated and perpendicular, R: round, C: clusters along the cell-laden hydrogel drop border. (D) The number of the A, P, R, C structures on BCC alone and BCC co-culture with MCC on day 5 (mean \pm s.e.m. $n = 261, 124$ structures). (E) The percentile distribution of the structures (χ^2 test). Horizontal bars show significant differences.

	BCC	BCC+MC	Significance*
R%	52	57	p>0.05
A%	23	5	p<0.05
P%	25	19	p>0.05
C%	0	19	p<0.05

Table 3.3. Significances of the changes in the individual percentiles of R, A, P, C structures of BCC cultured in collagen alone or in the presence of macrophages. *Two sample t-test between percents.

3.3.2. Macrophages reduced and promoted migration of BCC in matrigel and collagen, respectively

To determine cell migration in 3D in a controlled manner, we used a custom 3D co-culture cell-on-a-chip device, where we seeded BCC or macrophages alone or in combination in collagen or matrigel into a channel sided by channels containing cell-free hydrogels (Figure 3.14). In matrigel, BCC alone showed more migration than macrophages alone and presence of macrophages reduced the migration distance 2 fold on days 1, 3 and 5 ($p<0.028$). In collagen, BCC alone showed less migration than macrophages alone and presence of macrophages increased the migration distance 2.8 fold on day 5 ($p<1.54E-06$). Thus macrophages reduced and promoted migration of BCC in matrigel and collagen, respectively.

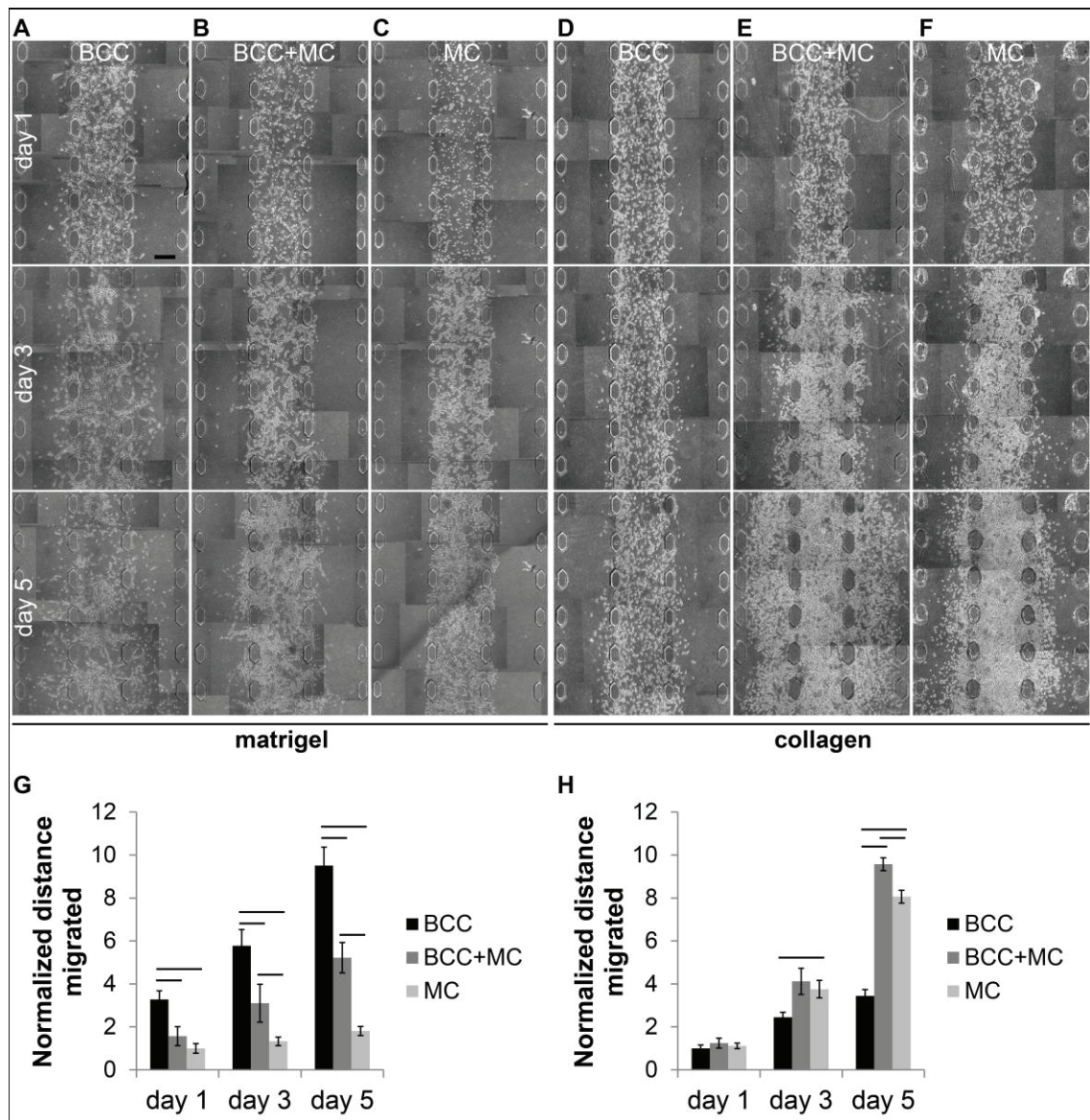


Figure 3.14. Macrophages reduced and promoted migration of BCC in matrigel and collagen, respectively.

(A) – (C) BCC alone, BCC and macrophages or macrophages alone in matrigel were loaded into the middle channel of a cell-on-a-chip device. (D) – (F) BCC alone, BCC and macrophages or macrophages alone in collagen were loaded into the middle channel of a cell-on-a-chip. Cell-free channels were loaded with the corresponding matrices. Quantification of distances migrated by cells in matrigel (G) and collagen (H) matrices (mean \pm s.e.m. $n=8$, 16 ROIs). Horizontal bars show significant differences between groups on the same day. (Scale bars, 250 μ m.)

3.4. Adherent but not suspended BCC endocytosed EGFR when in contact with macrophages

To confirm that juxtacrine signaling is the mechanism of interaction between macrophage-derived-EGF and BCC, we examined endocytosis of EGFR in BCC in

suspension and adherent cell culture (Figure 3.15 and Figure 3.16). When starved BCC were treated with BSA, EGF or macrophages in suspension, the fraction of membrane EGFR was the highest for BCC treated with macrophages than with BSA than with EGF ($p < 0.0015$) (Figure 3.15B). EGFR was expected to be internalized in the presence of macrophage-derived-EGF. Yet interactions of BCC with macrophages did not promote receptor internalization, which was probably because BCC in suspension did not have enough traction to disengage the macrophage-bound-EGF (Ivaska and Heino 2011). In adherent culture on the other hand, BCC cells transfected with EGFR-GFP starved and treated with macrophages endocytosed EGFR (69% of cells) more and less than those treated with BSA (11% of cells) and EGF (92% of cells), respectively ($\chi^2 p < 0.035$) (Figure 3.16B and Movie S1-S3) (APPENDIX B).

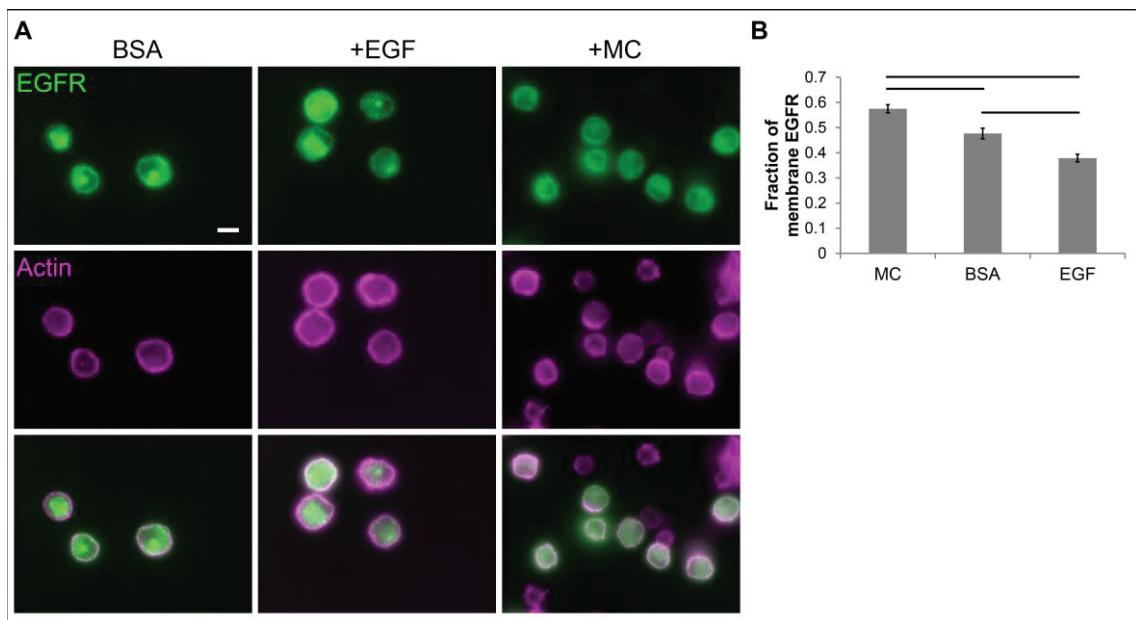


Figure 3.15. Endocytosis of EGFR in suspended BCC.

(A) Starved and suspended BCC were treated with BSA, EGF or macrophages for 15 minutes in suspension, fixed and stained. Representative immunostaining images for EGFR and actin localization. (Scale bars, 10 μm .) (B) The fraction of membrane EGFR derived from immunofluorescence signal (mean \pm s.e.m. $n = 35, 45, 27$ cells).

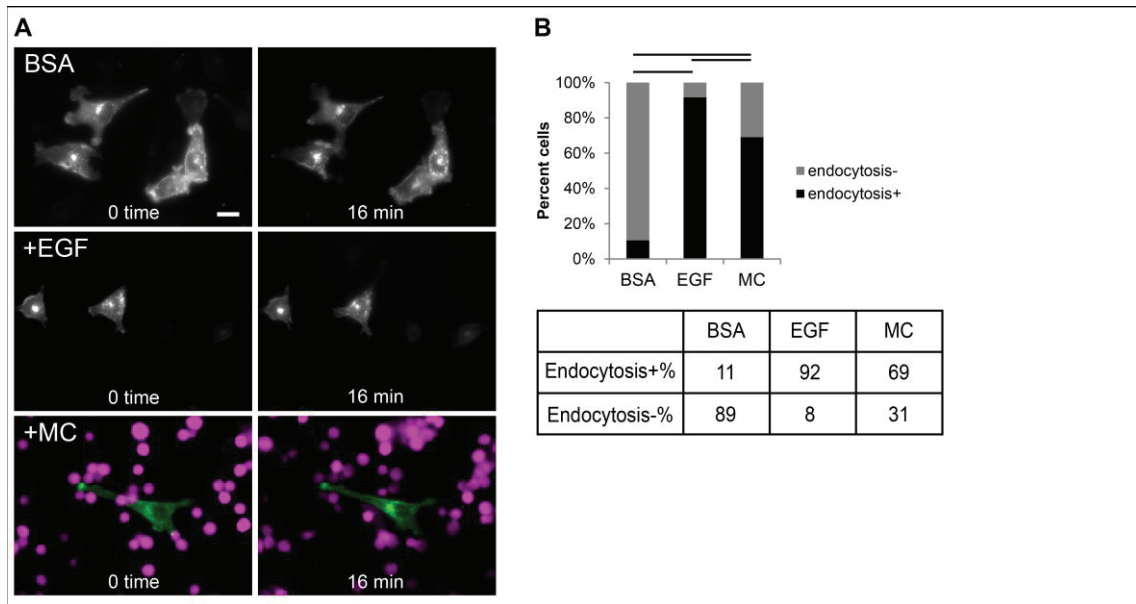


Figure 3.16. Adherent BCC endocytosed EGFR when in contact with macrophages.

(A) Representative images for 0th and 16th minute of live imaging of EGFR endocytosis in BCC transfected with EGFR-GFP, starved and treated with EGF or macrophages. (Scale bars, 10 μm .) (B) The percentage of the BCC cells showing EGFR endocytosis when treated with BSA, EGF or macrophages (χ^2 test for $n = 66, 24, 42$ cells). Horizontal bars show significant differences.

Although breast cancer cells (BCC) and macrophages are accepted to interact in a paracrine loop of epidermal growth factor (EGF) and colony stimulating factor-1, direct evidence to support this perception is lacking and the underlying mechanism of interaction remains unclear. We investigated the interaction between BCC and macrophages using a multidisciplinary approach. Our results support the hypothesis that a juxtacrine interaction is required for the activity of macrophage-derived-EGF on breast cancer cells, and thus the interaction between cancer cells and macrophages is a paracrine-juxtacrine loop of CSF-1 and EGF, respectively.

Growth factors can act either in soluble or ECM-bound or cell-bound (Singh and Harris 2005). Our first results showed that CSF-1 was secreted and thus a chemotactic response by macrophages towards BCC was possible and observed whereas EGF was not detected in the conditioned medium of macrophages and a chemotactic response by BCC to macrophage-derived-EGF was not observed. Secondly, we examined whether macrophage-derived-EGF could act as an ECM-bound growth factor. Here, we used mgel surfaces as positive controls. An important difference between mgel and MC surfaces was that unlike the latter, the former presented a rich ECM composition. Iressa decreased adhesion on mgel surfaces as expected since matrigel is a rich mixture of

ECM proteins and growth factors. Presence of EGF can promote adhesion via crosstalk between integrins and growth factor receptors and presence of iressa can remove the positive (pro-adhesion) input from EGFR (Comoglio, Boccaccio, and Trusolino 2003, Eliceiri 2001, Kim et al. 2008, Yamada and Even-Ram 2002). EGF is also known to promote motility. Macrophages appeared to inhibit cell adhesion and presence of iressa removed the negative (pro-motility) input from EGFR. This result was in agreement with the previous studies which found that EGF can promote rounding of adherent cells (Welsh et al. 1991), inhibit adhesion (Maheshwari et al. 1999) and promote a motile phenotype (Xie et al. 1998).

Adhesion of MDA-MB-231 cells, used here as a model for BCC, on collagen IV has been shown to increase in the presence of EGF and this increase can be reverted by EGFR inhibitors (Genersch et al. 1998). However, we cannot directly compare our results with those reported in that study because in our experimental system, soluble EGF is not present. Our results collectively indicated that macrophage-derived-EGF was cell-bound. On the other hand, in that study EGF has been shown to inhibit adhesion for cells with high EGFR expression. Thus it appears that the form of EGF – soluble or immobilized – and the number of EGFR per cell can modulate the effect of EGF on cell adhesion.

Iressa dependent differences on adhesion and motility were observed on macrophages but not on macrophage-derived-ECM, directing us to the investigation of cell-to-cell contact based interactions. In matrigel hydrogel drops, in the presence of macrophages, the number and percentage of branched structures decreased and the percentage of line structures increased suggesting that macrophages could induce a more dispersed organization of BCC. On the other hand, changes in the single and multi-cellular organization in collagen suggested that BCC and macrophages could cluster in a poor microenvironment such as collagen.

In 3D co-culture cell-on-a-chip devices, macrophages reduced and promoted migration of BCC in matrigel and collagen, respectively. In matrigel, BCC alone could migrate well due to the rich composition of matrigel which can activate both integrins and growth factor receptors; yet as BCC encountered macrophages which acted as concentrated point sources of EGF, they migrated less. This was probably because local EGF, that was the sum of EGF present in matrigel plus macrophage-derived-EGF, became too high and inhibited migration of BCC, consistent with biphasic EGF dependence of EGFR auto-phosphorylation (Needham et al. 2016) and results of *in vivo*

invasion assays performed with microneedles stably inserted into xenograft tumors in mice (Philippart et al. 2008). On the other hand, in 3D co-culture cell-on-a-chip devices comprising collagen, BCC alone did not migrate as well due to the poor composition of collagen; yet in this case interactions with macrophages, which acted as rich sources of EGF, promoted cell migration, as expected. Our 3D migration results for cells in collagen in custom cell-on-a-chip devices are also in agreement with previous studies where dissemination of tumor cells is induced by contact with macrophages (Bai et al. 2015, Goswami et al. 2005). Direct contact with macrophages is also known to induce other changes in cancer cells, such as formation of more invadopodia, which EGF is known to enhance (Roh-Johnson et al. 2014).

Our results on endocytosis of EGFR in suspension BCC when stimulated with macrophages are consistent with those of a study where cells were stimulated with surface immobilized EGF which has been suggested to be useful for studying juxtacrine signaling (Chen, Ito, and Imanishi 1997). Furthermore, our results on endocytosis of EGFR in adherent BCC when stimulated with macrophages align with those of a study where cells were stimulated with EGF-beads (Verveer et al. 2000).

CHAPTER 4

CONCLUSION

EGF – CSF-1 based interactions between cancer cells and macrophages have long been perceived as a paracrine loop. Using a multidisciplinary approach, our results revealed that cell-to-cell contact was required for the activity of macrophage-derived-EGF on BCC. To the best of our knowledge, this is the first study providing direct evidence and showing that the mechanism of interaction between macrophage-derived-EGF and BCC is juxtacrine signaling. The paradigm shift we provide is likely to promote a better understanding of cell-to-cell communication in both health and disease states, and well-designed cellular microenvironments to control and assay cell-to-cell interactions in tissue engineering applications and finally better therapeutic and diagnostic approaches in the future.

REFERENCES

- Alphonso, A., and S. K. Alahari. 2009. "Stromal cells and integrins: conforming to the needs of the tumor microenvironment." *Neoplasia* 11 (12):1264-71.
- Au, S. H., B. D. Storey, J. C. Moore, Q. Tang, Y. L. Chen, S. Javaid, A. F. Sarioglu, R. Sullivan, M. W. Madden, R. O'Keefe, D. A. Haber, S. Maheswaran, D. M. Langenau, S. L. Stott, and M. Toner. 2016. "Clusters of circulating tumor cells traverse capillary-sized vessels." *Proceedings of the National Academy of Sciences of the United States of America* 113 (18):4947-4952. doi: 10.1073/pnas.1524448113.
- Aznavoorian, S., M. L. Stracke, H. Krutzsch, E. Schiffmann, and L. A. Liotta. 1990. "Signal transduction for chemotaxis and haptotaxis by matrix molecules in tumor cells." *J Cell Biol* 110 (4):1427-38.
- Bai, J., G. Adriani, T. M. Dang, T. Y. Tu, H. X. Penny, S. C. Wong, R. D. Kamm, and J. P. Thiery. 2015. "Contact-dependent carcinoma aggregate dispersion by M2a macrophages via ICAM-1 and beta2 integrin interactions." *Oncotarget* 6 (28):25295-307. doi: 10.18632/oncotarget.4716.
- Carpenter, G., and S. Cohen. 1990. "Epidermal growth factor." *J Biol Chem* 265 (14):7709-12.
- Cavalcanti-Adam, E. A., T. Volberg, A. Micoulet, H. Kessler, B. Geiger, and J. P. Spatz. 2007. "Cell spreading and focal adhesion dynamics are regulated by spacing of integrin ligands." *Biophys J* 92 (8):2964-74. doi: 10.1529/biophysj.106.089730.
- Chen, C. S., M. Mrksich, S. Huang, G. M. Whitesides, and D. E. Ingber. 1997. "Geometric control of cell life and death." *Science* 276 (5317):1425-8.
- Chen, G., Y. Ito, and Y. Imanishi. 1997. "Photo-immobilization of epidermal growth factor enhances its mitogenic effect by artificial juxtacrine signaling." *Biochim Biophys Acta* 1358 (2):200-8.
- Comoglio, P. M., C. Boccaccio, and L. Trusolino. 2003. "Interactions between growth factor receptors and adhesion molecules: breaking the rules." *Current Opinion in Cell Biology* 15 (5):565-571. doi: 10.1016/s0955-0674(03)00096-6.

- Condeelis, J., and J. W. Pollard. 2006. "Macrophages: obligate partners for tumor cell migration, invasion, and metastasis." *Cell* 124 (2):263-6. doi: 10.1016/j.cell.2006.01.007.
- Dickson, R. B., S. E. Bates, M. E. McManaway, and M. E. Lippman. 1986. "Characterization of estrogen responsive transforming activity in human breast cancer cell lines." *Cancer Res* 46 (4 Pt 1):1707-13.
- Eliceiri, B. P. 2001. "Integrin and growth factor receptor crosstalk." *Circulation Research* 89 (12):1104-1110. doi: 10.1161/hh2401.101084.
- Genersch, E., D. W. Schneider, G. Sauer, K. Khazaie, D. Schuppan, and R. B. Lichtner. 1998. "Prevention of EGF-modulated adhesion of tumor cells to matrix proteins by specific EGF receptor inhibition." *Int J Cancer* 75 (2):205-9.
- Goswami, S., E. Sahai, J. B. Wyckoff, M. Cammer, D. Cox, F. J. Pixley, E. R. Stanley, J. E. Segall, and J. S. Condeelis. 2005. "Macrophages promote the invasion of breast carcinoma cells via a colony-stimulating factor-1/epidermal growth factor paracrine loop." *Cancer Res* 65 (12):5278-83. doi: 10.1158/0008-5472.can-04-1853.
- Gupta, G. P., and J. Massague. 2006. "Cancer metastasis: building a framework." *Cell* 127 (4):679-95. doi: 10.1016/j.cell.2006.11.001.
- Harris, R. C., E. Chung, and R. J. Coffey. 2003. "EGF receptor ligands." *Exp Cell Res* 284 (1):2-13.
- Hu, M., and K. Polyak. 2008. "Microenvironmental regulation of cancer development." *Curr Opin Genet Dev* 18 (1):27-34. doi: 10.1016/j.gde.2007.12.006.
- Huh, D., B. D. Matthews, A. Mammoto, M. Montoya-Zavala, H. Y. Hsin, and D. E. Ingber. 2010. "Reconstituting Organ-Level Lung Functions on a Chip." *Science* 328 (5986):1662-1668. doi: 10.1126/science.1188302.
- Ivaska, J., and J. Heino. 2011. "Cooperation between integrins and growth factor receptors in signaling and endocytosis." *Annu Rev Cell Dev Biol* 27:291-320. doi: 10.1146/annurev-cellbio-092910-154017.
- Iwamoto, R., K. Handa, and E. Mekada. 1999. "Contact-dependent growth inhibition and apoptosis of epidermal growth factor (EGF) receptor-expressing cells by the membrane-anchored form of heparin-binding EGF-like growth factor." *J Biol Chem* 274 (36):25906-12.

- Jeon, J. S., S. Bersini, M. Gilardi, G. Dubini, J. L. Charest, M. Moretti, and R. D. Kamm. 2015. "Human 3D vascularized organotypic microfluidic assays to study breast cancer cell extravasation." *Proceedings of the National Academy of Sciences of the United States of America* 112 (1):214-219. doi: 10.1073/pnas.1417115112.
- Keenan, T. M., and A. Folch. 2008. "Biomolecular gradients in cell culture systems." *Lab on a Chip* 8 (1):34-57. doi: 10.1039/b711887b.
- Kenny, P. A., and M. J. Bissell. 2003. "Tumor reversion: correction of malignant behavior by microenvironmental cues." *Int J Cancer* 107 (5):688-95. doi: 10.1002/ijc.11491.
- Kim, H. D., T. W. Guo, A. P. Wu, A. Wells, F. B. Gertler, and D. A. Lauffenburger. 2008. "Epidermal growth factor-induced enhancement of glioblastoma cell migration in 3D arises from an intrinsic increase in speed but an extrinsic matrix- and proteolysis-dependent increase in persistence." *Mol Biol Cell* 19 (10):4249-59. doi: 10.1091/mbc.E08-05-0501.
- Knutsdottir, H., J. S. Condeelis, and E. Palsson. 2016. "3-D individual cell based computational modeling of tumor cell-macrophage paracrine signaling mediated by EGF and CSF-1 gradients." *Integrative Biology* 8 (1):104-119. doi: 10.1039/c5ib00201j.
- Lieleg, O., R. M. Baumgartel, and A. R. Bausch. 2009. "Selective filtering of particles by the extracellular matrix: an electrostatic bandpass." *Biophys J* 97 (6):1569-77. doi: 10.1016/j.bpj.2009.07.009.
- Liotta, L. A., and E. C. Kohn. 2001. "The microenvironment of the tumour-host interface." *Nature* 411 (6835):375-9. doi: 10.1038/35077241.
- Maheshwari, G., A. Wells, L. G. Griffith, and D. A. Lauffenburger. 1999. "Biophysical integration of effects of epidermal growth factor and fibronectin on fibroblast migration." *Biophys J* 76 (5):2814-23. doi: 10.1016/s0006-3495(99)77435-7.
- Marusyk, A., D. P. Tabassum, M. Janiszewska, A. E. Place, A. Trinh, A. I. Rozhok, S. Pyne, J. L. Guerriero, S. Shu, M. Ekram, A. Ishkin, D. P. Cahill, Y. Nikolsky, T. A. Chan, M. F. Rimawi, S. Hilsenbeck, R. Schiff, K. C. Osborne, A. Letai, and K. Polyak. 2016. "Spatial Proximity to Fibroblasts Impacts Molecular Features and Therapeutic Sensitivity of Breast Cancer Cells Influencing Clinical Outcomes." *Cancer Res.* doi: 10.1158/0008-5472.CAN-16-1457.
- Massague, J., and A. Pandiella. 1993. "MEMBRANE-ANCHORED GROWTH-FACTORS." *Annual Review of Biochemistry* 62:515-541.

- McMillin, D. W., J. Delmore, E. Weisberg, J. M. Negri, D. C. Geer, S. Klippel, N. Mitsiades, R. L. Schlossman, N. C. Munshi, A. L. Kung, J. D. Griffin, P. G. Richardson, K. C. Anderson, and C. S. Mitsiades. 2010. "Tumor cell-specific bioluminescence platform to identify stroma-induced changes to anticancer drug activity." *Nat Med* 16 (4):483-9. doi: 10.1038/nm.2112.
- Memon, A. A., B. S. Sorensen, P. Meldgaard, L. Fokdal, T. Thykjaer, and E. Nexø. 2006. "The relation between survival and expression of HER1 and HER2 depends on the expression of HER3 and HER4: a study in bladder cancer patients." *Br J Cancer* 94 (11):1703-9. doi: 10.1038/sj.bjc.6603154.
- Mendoza, M., and C. Khanna. 2009. "Revisiting the seed and soil in cancer metastasis." *Int J Biochem Cell Biol* 41 (7):1452-62. doi: 10.1016/j.biocel.2009.01.015.
- Mierke, C. T., D. P. Zitterbart, P. Kollmannsberger, C. Raupach, U. Schlotzer-Schrehardt, T. W. Goecke, J. Behrens, and B. Fabry. 2008. "Breakdown of the endothelial barrier function in tumor cell transmigration." *Biophys J* 94 (7):2832-46. doi: 10.1529/biophysj.107.113613.
- Needham, S. R., S. K. Roberts, A. Arkhipov, V. P. Mysore, C. J. Tynan, L. C. Zanetti-Domingues, E. T. Kim, V. Losasso, D. Korovesis, M. Hirsch, D. J. Rolfe, D. T. Clarke, M. D. Winn, A. Lajevardipour, A. H. A. Clayton, L. J. Pike, M. Perani, P. J. Parker, Y. B. Shan, D. E. Shaw, and M. L. Martin-Fernandez. 2016. "EGFR oligomerization organizes kinase-active dimers into competent signalling platforms." *Nature Communications* 7. doi: 10.1038/ncomms13307.
- Ozdil, B., S. Onal, T. Oruc, and D. Pesen Okvur. 2014. "Fabrication of 3D Controlled in vitro Microenvironments." *MethodsX* 1:60-6. doi: 10.1016/j.mex.2014.06.003.
- Paget, S. 1889. "The distribution of secondary growths in cancer of the breast. 1889." *Cancer Metastasis Rev* 8 (2):98-101.
- Pesen, D., and D. B. Haviland. 2009. "Modulation of cell adhesion complexes by surface protein patterns." *ACS Appl Mater Interfaces* 1 (3):543-8. doi: 10.1021/am800264h.
- Philippar, U., E. T. Roussos, M. Oser, H. Yamaguchi, H. D. Kim, S. Giampieri, Y. R. Wang, S. Goswami, J. B. Wyckoff, D. A. Lauffenburger, E. Sahai, J. S. Condeelis, and F. B. Gertler. 2008. "A Mena Invasion Isoform Potentiates EGF-Induced Carcinoma Cell Invasion and Metastasis." *Developmental Cell* 15 (6):813-828. doi: 10.1016/j.devcel.2008.09.003.
- Pollard, J. W. 2004. "Tumour-educated macrophages promote tumour progression and metastasis." *Nat Rev Cancer* 4 (1):71-8. doi: 10.1038/nrc1256.

- Qin, D., Y. Xia, and G. M. Whitesides. 2010. "Soft lithography for micro- and nanoscale patterning." *Nat Protoc* 5 (3):491-502. doi: 10.1038/nprot.2009.234.
- Quail, D. F., and J. A. Joyce. 2013. "Microenvironmental regulation of tumor progression and metastasis." *Nat Med* 19 (11):1423-37. doi: 10.1038/nm.3394.
- Roh-Johnson, M., J. J. Bravo-Cordero, A. Patsialou, V. P. Sharma, P. Guo, H. Liu, L. Hodgson, and J. Condeelis. 2014. "Macrophage contact induces RhoA GTPase signaling to trigger tumor cell intravasation." *Oncogene* 33 (33):4203-12. doi: 10.1038/onc.2013.377.
- Sainsbury, J. R., A. J. Malcolm, D. R. Appleton, J. R. Farndon, and A. L. Harris. 1985. "Presence of epidermal growth factor receptor as an indicator of poor prognosis in patients with breast cancer." *J Clin Pathol* 38 (11):1225-8.
- Singh, A. B., and R. C. Harris. 2005. "Autocrine, paracrine and juxtacrine signaling by EGFR ligands." *Cellular Signalling* 17 (10):1183-1193.
- Singh, A. B., T. Tsukada, R. Zent, and R. C. Harris. 2004. "Membrane-associated HB-EGF modulates HGF-induced cellular responses in MDCK cells." *J Cell Sci* 117 (Pt 8):1365-79. doi: 10.1242/jcs.01037.
- Studebaker, A. W., G. Storci, J. L. Werbeck, P. Sansone, A. K. Sasser, S. Tavorari, T. Huang, M. W. Chan, F. C. Marini, T. J. Rosol, M. Bonafe, and B. M. Hall. 2008. "Fibroblasts isolated from common sites of breast cancer metastasis enhance cancer cell growth rates and invasiveness in an interleukin-6-dependent manner." *Cancer Res* 68 (21):9087-95. doi: 10.1158/0008-5472.can-08-0400.
- Taipale, J., and J. KeskiOja. 1997. "Growth factors in the extracellular matrix." *Faseb Journal* 11 (1):51-59.
- They, M., V. Racine, A. Pepin, M. Piel, Y. Chen, J. B. Sibarita, and M. Bornens. 2005. "The extracellular matrix guides the orientation of the cell division axis." *Nat Cell Biol* 7 (10):947-53. doi: 10.1038/ncb1307.
- Verveer, P. J., F. S. Wouters, A. R. Reynolds, and P. I. H. Bastiaens. 2000. "Quantitative imaging of lateral ErbB1 receptor signal propagation in the plasma membrane." *Science* 290 (5496):1567-1570. doi: 10.1126/science.290.5496.1567.
- Vlaicu, P., P. Mertins, T. Mayr, P. Widschwendter, B. Ataseven, B. Hogel, W. Eiermann, P. Knyazev, and A. Ullrich. 2013. "Monocytes/macrophages support

mammary tumor invasivity by co-secreting lineage-specific EGFR ligands and a STAT3 activator." *Bmc Cancer* 13. doi: 10.1186/1471-2407-13-197.

- Wakeling, A. E., S. P. Guy, J. R. Woodburn, S. E. Ashton, B. J. Curry, A. J. Barker, and K. H. Gibson. 2002. "ZD1839 (Iressa): an orally active inhibitor of epidermal growth factor signaling with potential for cancer therapy." *Cancer Res* 62 (20):5749-54.
- Ward, R., A. H. Sims, A. Lee, C. Lo, L. Wynne, H. Yusuf, H. Gregson, M. P. Lisanti, F. Sotgia, G. Landberg, and R. Lamb. 2015. "Monocytes and macrophages, implications for breast cancer migration and stem cell-like activity and treatment." *Oncotarget* 6 (16):14687-99. doi: 10.18632/oncotarget.4189.
- Weaver, V. M., O. W. Petersen, F. Wang, C. A. Larabell, P. Briand, C. Damsky, and M. J. Bissell. 1997. "Reversion of the malignant phenotype of human breast cells in three-dimensional culture and in vivo by integrin blocking antibodies." *J Cell Biol* 137 (1):231-45.
- Welsh, J. B., G. N. Gill, M. G. Rosenfeld, and A. Wells. 1991. "A negative feedback loop attenuates EGF-induced morphological changes." *J Cell Biol* 114 (3):533-43.
- Wolf, K., S. Alexander, V. Schacht, L. M. Coussens, U. H. von Andrian, J. van Rheenen, E. Deryugina, and P. Friedl. 2009. "Collagen-based cell migration models in vitro and in vivo." *Semin Cell Dev Biol* 20 (8):931-41. doi: 10.1016/j.semcdb.2009.08.005.
- Woodcock, J., and R. Woosley. 2008. "The FDA critical path initiative and its influence on new drug development." *Annu Rev Med* 59:1-12. doi: 10.1146/annurev.med.59.090506.155819.
- Wyckoff, J., W. G. Wang, E. Y. Lin, Y. R. Wang, F. Pixley, E. R. Stanley, T. Graf, J. W. Pollard, J. Segall, and J. Condeelis. 2004. "A paracrine loop between tumor cells and macrophages is required for tumor cell migration in mammary tumors." *Cancer Research* 64 (19):7022-7029. doi: 10.1158/0008-5472.can-04-1449.
- Xie, H., M. A. Pallerio, K. Gupta, P. Chang, M. F. Ware, W. Witke, D. J. Kwiatkowski, D. A. Lauffenburger, J. E. Murphy-Ullrich, and A. Wells. 1998. "EGF receptor regulation of cell motility: EGF induces disassembly of focal adhesions independently of the motility-associated PLCgamma signaling pathway." *J Cell Sci* 111 (Pt 5):615-24.

Yamada, K. M., and S. Even-Ram. 2002. "Integrin regulation of growth factor receptors." *Nature Cell Biology* 4 (4):E75-E76. doi: 10.1038/ncb0402-e75.

Young, E. W., and C. A. Simmons. 2010. "Macro- and microscale fluid flow systems for endothelial cell biology." *Lab Chip* 10 (2):143-60. doi: 10.1039/b913390a.

APPENDIX A

PUBLISHED ARTICLE

Fabrication of 3D Controlled in vitro Microenvironments,
doi:10.1016/j.mex.2014.06.003

APPENDIX B

SUPPLEMENTARY VIDEOS

Movie S1. EGFR endocytosis in BCC transfected with EGFR-GFP and starved.

Movie S2. EGFR endocytosis in BCC transfected with EGFR-GFP, starved and treated with EGF.

Movie S3. EGFR endocytosis in BCC transfected with EGFR-GFP, starved and treated with macrophages.

APPENDIX C

SUPPLEMENTARY DATASET

Excel S1. Descriptive statistics and statistical tests.

APPENDIX A

PUBLISHED ARTICLE

Fabrication of 3D Controlled in vitro Microenvironments,
doi:10.1016/j.mex.2014.06.003



Contents lists available at ScienceDirect

MethodsX

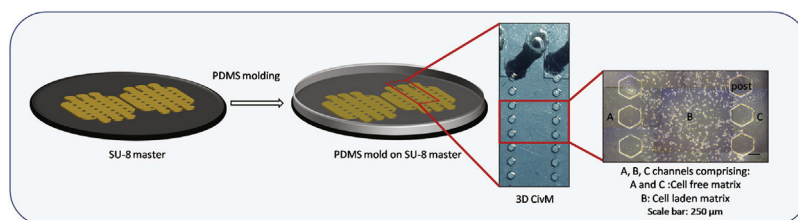
journal homepage: www.elsevier.com/locate/mex

Fabrication of 3D Controlled *in vitro* Microenvironments

Berrin Ozdil, Sevgi Onal, Tugce Oruc¹, Devrim Pesen Okvur^{*}

Izmir Institute of Technology, Department of Molecular Biology and Genetics, 35430 Izmir, Turkey

GRAPHICAL ABSTRACT



ABSTRACT

Microfluidics-based lab-on-a-chips have many advantages, one of which is to provide physiologically relevant settings for cell biology experiments. Thus there is an ever increasing interest in their fabrication. Our goal is to construct three dimensional (3D) Controlled *in vitro* Microenvironments (CivMs) that mimic the *in vivo* microenvironments. Here, we present our optimized fabrication method that works for various lab-on-a-chip designs with a wide range of dimensions. The most crucial points are:

- While using one type of SU-8 photoresist (SU-2075), fine tuning of ramp, dwell time, spin speed, durations of soft bake, UV exposure and development allows fabrication of SU-8 masters with various heights from 40 to 600 μm .
- Molding PDMS (polydimethylsiloxane) at room temperature for at least two days instead of baking at higher temperatures prevents not only tears and bubbles in PDMS stamps but also cracks in the SU-8 master.
- 3D nature of the CivMs is ensured by keeping the devices inverted during gel polymerization.

© 2014 The Authors. Published by Elsevier B.V. This is an open access article under the CC BY license (<http://creativecommons.org/licenses/by/3.0/>).

ARTICLE INFO

Method name: Fabrication of microfluidics based lab on a chips

Keywords: UV lithography, Polydimethylsiloxane, Microfluidic device, Lab-on-a-chip, Microenvironment, Hydrogel, Matrigel

Article history: Received 22 March 2014; Accepted 20 June 2014; Available online 9 July 2014

^{*} Corresponding author. Tel.: +90 2327507304.

E-mail address: devrimpesen@iyte.edu.tr (D. Pesen Okvur).

¹ Present address: Sabanci University, Department of Biological Sciences and Bioengineering, 34956 Istanbul, Turkey.

<http://dx.doi.org/10.1016/j.mex.2014.06.003>

2215-0161/© 2014 The Authors. Published by Elsevier B.V. This is an open access article under the CC BY license (<http://creativecommons.org/licenses/by/3.0/>).

Microfluidics-based lab-on-a-chips have many advantages [1]: Small volumes down to pL are used. Small volumes provide enhanced safety when dangerous or toxic chemicals or biological agents are used. Precise spatial and temporal control can be achieved. High throughput analysis is facilitated [2]. Fabrication costs are low. The devices are portable. Finally, the devices provide physiologically relevant settings for cell biology experiments [3–8]. Such advantages have resulted in an increased interest in the methodological details of fabrication of lab-on-a-chips [9–11].

Method details

UV lithography

UV lithography (UVL) which is also called photolithography is a parallel writing method for fabrication of 2D and 3D micrometer scale designs using photo-reactive materials, called photoresists [10]. There are two types of photoresists: Positive and negative. Positive photoresist is degraded by exposure to UV light followed by dissolution in a developer while negative photoresist such as SU-8, is cross-linked in the same process. SU-8 is widely used for fabrication of masters that are in turn used for both 2D and 3D structures of interest. SU-8 is an epoxy based negative photoresist. SU-8 is available in different viscosities and is categorized as SU-8 2000 and 3000 series. The higher the viscosity (and the number following 'SU-8'), the higher the thickness of the polymer spun on a surface. We fabricate SU-8 masters with heights between 40 and 600 μm using SU-8 2075. These masters can then be used for PDMS molding. PDMS molds in turn are used for fabricating 3D Controlled *in vitro* Microenvironments (CivMs). Some of our 3D microfluidic platforms have a set of microfluidic channels separated by an array of posts. Such systems are convenient for studying different hydrogels and cell types in the same device at predefined dimensions while mimicking *in vivo* conditions [2–5].

UV lithography is carried out in a Class 1000 clean room. Special lab overalls suited for clean room use are worn.

First improvement of our method is the ability to generate SU-8 layers with different thicknesses ranging from 40 to 600 microns using only SU-8 2075 through careful optimization of the steps of UV lithography, in particular the spinning step. Thus the users do not need to procure all different kinds of SU-8 in their laboratories.

Materials

Photoresist SU-8 2075 [!Caution: Wear protective gloves].

SU-8 developer (Stored at +4°C)

Si wafer

Acetone

Isopropanol

Dust-free tissue paper

Aluminum foil

Paper towel

Designed mask

Tweezers

Equipment

Hot plate

Mask aligner

Spin coater [!Caution: Do not open lid until the spinner comes to a full stop]

Fume hood

Stereoscopic microscope

Spin coating of SU-8

Day 1. First set the hot plate to 65°C at least half an hour beforehand to ensure uniform heating and place the SU-8 bottle on the bench so that its temperature equilibrates to room temperature.

A piece of aluminum foil should be placed on the hot plate before placing the wafer to avoid any photoresist residues contaminating the hot plate and to facilitate handling of the wafer. In addition, the tweezers used for handling SU-8 should not be used for handling other materials.

- Take a silicon wafer using tweezers from its package and leave it on the hot plate for approximately 5 min, then pick up the wafer with its aluminum foil and place it on the bench.
- Pour the SU-8 onto the wafer holding the SU-8 bottle very close to the wafer surface to prevent the formation of bubbles.

Slowly retract the SU-8 bottle by rotating it and place again in the hood but do not close its mouth with its cap. Loosely cover the mouth of the bottle with a piece of aluminum foil and wait until all the SU-8 moves back towards the bottom of the bottle. Any SU-8 remaining on the mouth of the bottle will crystallize in time and can interfere with a uniform SU-8 coating on the silicon wafer.

- Disperse the SU-8 on the wafer homogenously by gently moving the wafer at an angle in a circular motion. Avoid generating any bubbles or waves.
- Keep the wafer on the bench for approximately 10min so that it equilibrates to room temperature and the photoresist relaxes.

Relaxation of the photoresist can alternatively be carried out on the chuck of the spin coater. This ensures smaller temperature differences between the chuck and the sample and a homogenous surface during various spin rates.

- Cover the inner surface of the spin coater with aluminum foil beforehand to keep the spin coater clean.
- Use the proper recipe that will yield the desired thickness of the SU-8 layer.

For instance: For a final SU-8 thickness of 200 μm , perform the following steps:

*Ramp up to 500rpm in 5s, spin at 500rpm for 5s,
ramp up to 1000rpm in 5s, spin at 1000rpm for 20s,
ramp down to 500rpm in 5s, spin 500rpm for 5s,
ramp down to 0rpm in 5s.*

- Wait until the spinner comes to a full stop before opening the lid.
- Remove the wafer from the spin coater and place it on a piece of aluminum foil on the bench to allow for the relaxation of photoresist. Any waves present will slowly disappear.
- Place the wafer with its aluminum foil on the hot plate set to 65 °C for 20min. Then increase the temperature to 95 °C and leave the wafer at this temperature for 5 h. This is the soft bake step. If thin SU-8 layers are prepared, 3–4h are enough.
- Dispose of the materials contaminated with SU-8 according to your institution's guidelines.

Exposure of the SU-8 coated wafer to UV light

Day 2. First set the hot plate to 95 °C at least half an hour beforehand to ensure uniform heating.

- To test whether any wrinkles will form and to confirm that the soft bake is complete, place the SU-8 coated wafer on the hot plate at 95 °C. If there are no wrinkles on the SU-8 surface, then the sample is ready for UV exposure. If wrinkles appear, place the SU-8 coated wafer on the bench for the relaxation of the photoresist for approximately 5 min and then re-place it on the hot plate for an additional bake of 10 min. Repeat these steps until no wrinkles form.
- Based on the power settings of the mask aligner, one can calculate the time for exposure for a desired final dose ($\text{mWatt/cm}^2 \text{ s} = \text{mJ/cm}^2$). For a setting of 8 mWatt/cm^2 , we used exposure times up to 60 s.
- Adjust the time of the exposure to 60s for an SU-8 thickness of about 400 μm , and to 30s for thicknesses less than 200 μm . Here, SU-8 is intentionally overexposed to facilitate PDMS removal in

later steps. However, too much overexposure will prevent the proper development of the SU-8 pattern.

- Place the SU-8 coated wafer on the mask aligner stage. Then place the acetate film mask on the wafer. The opaque surface of the mask should face the SU-8 layer.
- After UV exposure is completed, place the sample on the bench for 5 min for relaxation of the photoresist.
- Place the sample on the hot plate set at 65 °C for 5 min, then increase the temperature to 95 °C and leave the wafer at this temperature for about 15 min. This is the post bake step. Turn off the hot plate and leave the sample on the hot plate to let it cool down slowly to room temperature.

Development of the SU-8 master

Day 3.

- Place the SU-8 developer and isopropanol on the bench so that they equilibrate to room temperature.
- Keep the SU-8 master in a petri dish filled with developer for 5 min without shaking. Then shake the sample in the developer for 15 min. After this, dispose of the developer. Shake SU-8 master in a fresh volume of developer again for 20 min. The UV exposed parts of SU-8 will remain on the wafer and the unexposed parts will be washed away.

If the pattern has posts (pillars) on a thin SU-8 layer, treat the sample with SU-8 developer for 10–15 min, i.e. shorter durations, and check that all the pillars are developed well under a stereo microscope with a UV filter. Even if only one pillar region is not open (developed), this may cause absence of a PDMS post in turn and thus leakage of the hydrogels through the adjacent channels during the CivMs experiments.

- Apply the isopropanol (IP) test. When a few drops of IP are applied on a small part of the SU-8 sample, usually the corner of a pattern, a white precipitate will form if the SU-8 is under-developed. If this is the case, shake the sample again in a fresh volume of developer. If the sample is well-developed, i.e. there is no white precipitate, hold the sample vertically and wash it 10 times with developer to remove any remaining small SU-8 particles on the wafer, and then wash it 10 times with IP which stops the development.
- Dry the SU-8 master with dust-free tissue paper. The SU-8 master is now ready.
- Wash the petri dishes and tweezers with acetone, IP and finally with H₂O.

Remember that SU-8 is sensitive to light. All the applications on the wafer with SU-8 should be performed in a clean room which is illuminated with yellow light. After the SU-8 master is ready, it can be handled in a standard laboratory.

PDMS molding

Second improvement of our method is for PDMS molding through room temperature polymerization, which not only preserves the SU-8 masters for years but also prevents damage to the resulting PDMS molds.

Materials

Sylgard 184 silicone elastomer base and curing agent
Demolding agent: Triton-X-100:H₂O:Absolute EtOH 1:9:40
Plastic cups and spoons
Aluminum foil and paper towel

Equipment

Balance
Vacuum desiccator

PDMS is provided as base and curing agent. The typical ratio for mixing is 10:1. A 5:1 ratio results in a stiffer PDMS.

- Determine the final weight of PDMS needed and calculate the required weight for base and curing agent. Weigh the base first and then add the appropriate amount of curing agent which is easier to weight. For a four inch wafer, a total of 30g of PDMS is sufficient.
- Mix the base and curing agent well.

The high number of bubbles reflects how good the base is mixed with the curing agent.

- Degas the mixture to remove all the bubbles by placing the mixture in a desiccator coupled to vacuum for 2×10 min.
- In the meantime, wash the SU-8 master with EtOH (70%), and H₂O. Then clean it with the demolding agent (cleaning buffer). Demolding agent provides easy separation of PDMS mold from the SU-8 master in later steps.
- Use a 10 cm glass petri dish to shape a piece of aluminum foil into a shallow container. Place a piece of double sticky tape in the middle and place the SU-8 master inside.
- Pour the degassed PDMS mixture onto the SU-8 master.
- Leave the PDMS mixture on a uniformly level surface for polymerization at room temperature for at least 2 days.

If the PDMS mixture on the SU-8 master is baked just after it is poured on the wafer, any possible bubbles generated during the pouring of the PDMS mixture will be fixed in the PDMS and the SU-8 master will be more likely to crack.

- After at least 2 days, separate the polymerized PDMS from the wafer.

Applying EtOH at the PDMS – SU-8 interface helps removal.

Construction of 3D Controlled *in vitro* Microenvironments (CivMs)

Construction of 3D Controlled *in vitro* Microenvironments needs to be preceded with the fabrication of SU-8 masters and molding of PDMS. Bonding of glass slides and PDMS molds is required for the completion of the 3D devices. Fabricated devices should be well sterilized to prevent any contamination that may hinder the biological application. SU-8 masters are reusable while the devices themselves can also be cleaned and reused although this is neither required nor recommended.

Third improvement of our method is that keeping the devices inverted during gel polymerization ensures a truly 3D distribution of cells in the matrix. Otherwise cells sink the bottom glass surface and show a 2D phenotype. In addition, we provide a detailed procedure for a rather neglected step of cleaning of the PDMS molds as well cleaned PDMS molds are essential for proper formation of 3D microenvironments that are devoid of any contaminants.

Materials

Glass slides
Scotch tape
70% EtOH
Deionized water (H₂O)
Matrigel

Equipment

Sonicator
UV/Ozone Plasma Cleaner [!Caution: Do not inhale the gases generated during the process].
Hot plate

Preparation of PDMS molds

- Cut out the PDMS molds along their borders and punch holes at proper positions for inlets and outlets.
- Use Scotch tape to remove any dust from the PDMS surfaces.
- Holding the PDMS molds with plastic tweezers, wash them with H₂O several times and place them into glass containers such as beakers.
- Sonicate in H₂O for 10 min; rinse with H₂O 5 times.
- Sonicate in 70% EtOH for 5 min; rinse with 70% EtOH twice.
- Keep in 70% EtOH for 5 min on bench.
- Place the samples inside a laminar hood, rinse with H₂O once and aspirate any liquid left on or inside the samples.
- After the PDMS molds are dry, place them into an autoclaved petri dish; the patterned sides of the PDMS molds should be facing up. Cover the petri dish with aluminum foil.
- Keep these samples at room temperature for 2 days so that they are completely dry as the next step is bonding and the samples that will be treated in UV/ozone plasma should be completely dry.

Permanent bonding of 3D CivMs

- Treat a clean slide and a PDMS mold in the UV/ozone cleaner for 5 min. Then immediately bond the treated surfaces facing each other to obtain the complete 3D CivMs.

At each UV/ozone treatment, clean one slide and one PDMS mold as the bonding step should be done immediately without losing the effect of the UV/ozone treatment.

- Place the 3D CivMs on the hot plate at nearly 100 °C for at least 10 min and cover them with elevated aluminum foil pieces to create an oven effect, to protect from dust and to ensure permanent bonding of the PDMS molds with the slides.
- Turn off the hot plate and let the 3D CivMs cool down to room temperature.

Sterilization of 3D CivMs

- Rinse all inside and outside surfaces of the 3D CivMs and the petri dish with 70% EtOH and take them into a laminar flow hood.
- Aspirate any liquid on or inside the 3D CivMs and wash inside the channels with autoclaved H₂O twice.
- Aspirate any liquid on or inside the 3D CivMs and place them into a new autoclaved petri dish.
- Let the samples dry and expose them to UV light for 30 min.
- Place the 3D CivMs inside the petri dish covered with aluminum foil in an oven and heat the samples at 80 °C for 24 h for restoration of hydrophobicity.

During UV/ozone treatment, the PDMS and glass slide surfaces become hydrophilic. In order to make them hydrophobic again, and thus, prevent the leakage of the hydrogels through the adjacent microchannels during loading, the samples are heated at 80 °C for at least 24 h (4). Once this heating process is completed, the samples are ready for loading of the hydrogels.

Loading of 3D CivMs with hydrogels

- Mix Matrigel with cell suspension at 1:1 ratio on ice.

A rack made of aluminum placed on ice is very useful for holding tubes at a constant and cold temperature of +4 °C.

Matrigel is normally stored at –80 °C. Thaw the matrigel overnight within ice bath at +4 °C. Other hydrogels such as collagen can also be used instead of matrigel.

- Place the 3D CivMs directly on 70% EtOH soaked sterile filter paper placed on an aluminum block in contact with an ice bath.

If the 3D CivMs are not cold, matrigel will start to polymerize upon contact and loading can be compromised.

- Load the cell laden Matrigel to the corresponding channel with a 200 μ l-pipette and allow for polymerization at room temperature for 30 min. Invert the samples to prevent cells from sinking to the bottom glass surface.

While loading the gels, hold the sample vertically and work slowly to prevent the gel of interest from passing through pillar regions to other channels. Inverting the 3D CivMs just after loading a (cell-laden) matrix makes the borders of gels more defined and ensures that cells do not precipitate to the bottom of the device.

- After gel loading and polymerization are complete, add culture media into the medium reservoirs.
- Place the 3D CivMs into new sterile petri dishes and place open microcentrifuge tubes filled with autoclaved H₂O to minimize the evaporation of medium from the devices. Also close inlets and outlets of the gel channels with PDMS pieces to minimize evaporation.
- Keep the samples at 37 °C and 5% CO₂ or other cell culture conditions required by the cells.
- Collect data on cell behavior, for example, by taking phase contrast or fluorescence images of cells in 3D CivMs every day. Once image data are collected, Photoshop and/or ImageJ can be used for image processing and analysis.

Acknowledgements

This work was supported by FP7 Marie Curie Grant PIRG08-GA-2010-27697 and IYTE Scientific Research Project 2011IYTE25. Samples were fabricated in the IYTE Applied Quantum Research Center, supported by DPT (State Planning Organization) Grant 2009K120860. MethodsX thanks the anonymous reviewers of this article for taking the time to provide valuable feedback.

References

- [1] E.K. Sackmann, A.L. Fulton, D.J. Beebe, The present and future role of microfluidics in biomedical research, *Nature* 507 (March (7491)) (2014) 181–189, PubMed PMID: WOS:000332651800029.
- [2] C.Y. Li, D.K. Wood, J.H. Huang, S.N. Bhatia, Flow-based pipeline for systematic modulation and analysis of 3D tumor microenvironments, *Lab on a Chip* 13 (10) (2013) 1969–1978, PubMed PMID: WOS:000317937300018.
- [3] K. Funamoto, I.K. Zervantonakis, Y.C. Liu, C.J. Ochs, C. Kim, R.D. Kamm, A novel microfluidic platform for high-resolution imaging of a three-dimensional cell culture under a controlled hypoxic environment, *Lab on a Chip* 12 (November (22)) (2012) 4855–4863, PubMed PMID: WOS:000310865200035.
- [4] U. Haessler, J.C. Teo, D. Foretay, P. Renaud, M.A. Swartz, Migration dynamics of breast cancer cells in a tunable 3D interstitial flow chamber, *Integr. Biol.* 4 (April (4)) (2012) 401–409, PubMed PMID: 22143066 (Epub 2011/12/07).
- [5] H.Y. Hsieh, G. Camci-Unal, T.W. Huang, R. Liao, T.J. Chen, A. Paul, et al., Gradient static-strain stimulation in a microfluidic chip for 3D cellular alignment, *Lab on a Chip* 14 (3) (2014) 482–493, PubMed PMID: WOS:000328911400005.
- [6] C.P. Huang, J. Lu, H. Seon, A.P. Lee, L.A. Flanagan, H.Y. Kim, et al., Engineering microscale cellular niches for three-dimensional multicellular co-cultures, *Lab on a Chip* 9 (June (12)) (2009) 1740–1748, PubMed PMID: 19495458. Pubmed Central PMCID: Pmc3758562 (Epub 2009/06/06).
- [7] A.P. Wong, R. Perez-Castillejos, J. Christopher Love, G.M. Whitesides, Partitioning microfluidic channels with hydrogel to construct tunable 3-D cellular microenvironments, *Biomaterials* 29 (April (12)) (2008) 1853–1861, PubMed PMID: 18243301. Pubmed Central PMCID: Pmc2288785 (Epub 2008/02/05).
- [8] I.K. Zervantonakis, S.K. Hughes-Alford, J.L. Charest, J.S. Condeelis, F.B. Gertler, R.D. Kamm, Three-dimensional microfluidic model for tumor cell intravasation and endothelial barrier function, *Proc. Natl. Acad. Sci. U. S. A.* 109 (August (34)) (2012) 13515–13520, PubMed PMID: 22869695. Pubmed Central PMCID: Pmc3427099 (Epub 2012/08/08).
- [9] W.N. Bian, B. Liao, N. Badie, N. Bursac, Mesoscopic hydrogel molding to control the 3D geometry of bioartificial muscle tissues, *Nat. Protoc.* 4 (10) (2009) 1522–1534, PubMed PMID: WOS:000275367400011.
- [10] D. Qin, Y. Xia, G.M. Whitesides, Soft lithography for micro- and nanoscale patterning, *Nat. Protoc.* 5 (March (3)) (2010) 491–502, PubMed PMID: 20203666 (Epub 2010/03/06).
- [11] Y. Shin, S. Han, J.S. Jeon, K. Yamamoto, I.K. Zervantonakis, R. Sudo, et al., Microfluidic assay for simultaneous culture of multiple cell types on surfaces or within hydrogels, *Nat. Protoc.* 7 (July (7)) (2012) 1247–1259, PubMed PMID: 22678430 (Epub 2012/06/09).

APPENDIX B

SUPPLEMENTARY VIDEOS

Movie S1. EGFR endocytosis in BCC transfected with EGFR-GFP and starved.

Movie S2. EGFR endocytosis in BCC transfected with EGFR-GFP, starved and treated with EGF.

Movie S3. EGFR endocytosis in BCC transfected with EGFR-GFP, starved and treated with macrophages.

Movies are available at the following link:

<https://yadi.sk/d/z-N-dayF3Gp2n7>

APPENDIX C

SUPPLEMENTARY DATASET

Excel S1. Descriptive statistics and statistical tests.

FIG 3.2A

	Mgel0'	Mgel10'	Mgel20'	Mgel30'	Mgel40'	Mgel50'	MCm0'	MCm10'	MCm20'	MCm30'	MCm40'	MCm50'	MCD'	MCn10'	MCn20'	MCn30'	MCn40'	MCn50'	MC30'	MC40'	MC50'	G0'	G10'	G20'	G30'	G40'	G50'	
Mgel0'	NaN																											
Mgel10'	2.19E-05	1																										
Mgel20'	0.2481687		1																									
Mgel30'	0.1891823			1																								
Mgel40'	0.1495993				1																							
Mgel50'	0.132882					1																						
MCm0'	2.36E-06	2.36E-06	2.36E-06	2.36E-06	2.36E-06	NaN																						
MCm10'	0.1566211	7.74E-05	5.04E-05	5.61E-05	5.61E-05	0.1150869	1																					
MCm20'	0.6431134	0.0001776	8.61E-05	0.0001307	6.96E-05	0.6044791	0.9753258	1																				
MCm30'	1	0.000758	0.0001178	0.0002172	0.0001776	9.56E-05	1	0.9917741																				
MCm40'	0.6431134	0.0018487	0.0003556	0.0005733	0.0003226	0.6044791	0.4036637	0.4153722	1																			
MCm50'	0.3472489	0.0028226	0.000758	0.0006297	0.0005217	0.0002651	0.2951175	0.2524616	0.2198717	0.3376525	0.7028593	1																
MC10'	0.2218103	3.39E-06	3.39E-06	3.39E-06	3.39E-06	NaN	0.1208126	0.6103494	1	0.6103494	0.3027879	NaN	0.1807111															
MC20'	0.0681783	1.75E-05	2.48E-05	1.96E-05	3.93E-05	1.22E-05	0.173866	0.9068222	0.8915101	0.7095766	0.3657515	0.3545803	0.1807111	1														
MC30'	0.4668914	1.08E-05	1.08E-05	1.22E-05	2.48E-05	1.08E-05	0.4171586	0.5441693	0.4628215	0.2548886	0.0906703	0.1177744	0.4246126	0.6288671	0.8090429	1												
MC40'	0.8154788	4.56E-06	8.47E-06	4.02E-06	1.75E-05	4.56E-06	0.7926776	0.3436271	0.2461152	0.2054257	0.0625857	0.0688259	0.7961597	0.4162985	0.7252081	0.5530688	1											
MC50'	0.8154788	7.50E-06	7.50E-06	2.48E-05	4.02E-06	0.0053041	0.0053041	NaN	0.4372935	0.4005632	0.1335264	0.1281041	0.7961597	0.5384642	0.8090429	0.8432621	0.775185	1										
G0'	0.0053041	0.0053041	0.0053041	0.0053041	0.0053041	NaN	0.3623555	0.7746649	1	0.7746649	0.5494515	NaN	0.4330163	0.2676584	0.6457962	0.89247	0.89247	1										
G10'	0.1251198	0.0056633	0.0056633	0.0056633	0.0037316	0.004246	0.5169236	0.659427	1	0.8155175	0.7361099	0.087156	0.7263775	0.4350062	0.9785243	0.8505367	0.7263775	0.3636364	1									
G20'	0.001864	0.0056633	0.0056633	0.0056633	0.004246	0.5169236	0.659427	1	0.8155175	0.7361099	0.087156	0.7263775	0.4350062	0.9785243	0.8505367	0.7263775	0.3636364	0.047619	1									
G30'	0.1251198	0.0056633	0.0056633	0.0056633	0.0037316	0.004246	0.5169236	0.659427	1	0.8155175	0.7361099	0.087156	0.7263775	0.4350062	0.9785243	0.8505367	0.7263775	0.3636364	0.047619	1								
G40'	0.1251198	0.0056633	0.0056633	0.0056633	0.0037316	0.004246	0.5169236	0.659427	1	0.8155175	0.7361099	0.087156	0.7263775	0.4350062	0.9785243	0.8505367	0.7263775	0.3636364	0.047619	1								
G50'	0.001864	0.0056633	0.0056633	0.0056633	0.004246	0.5169236	0.659427	1	0.8155175	0.7361099	0.087156	0.7263775	0.4350062	0.9785243	0.8505367	0.7263775	0.3636364	0.047619	1									

	Mgel0'	Mgel10'	Mgel20'	Mgel30'	Mgel40'	Mgel50'	MCm0'	MCm10'	MCm20'	MCm30'	MCm40'	MCm50'	MCD'	MCn10'	MCn20'	MCn30'	MCn40'	MCn50'	MC30'	MC40'	MC50'	G0'	G10'	G20'	G30'	G40'	G50'
mean	1.29248713	4.0262074	4.3942051	4.6209593	4.7920124		1.1064659	1.1897673	1.2996728	1.3736955	1.4748476		1.0507116	1.016347	1.0289771	1.0061636	1.0133083	1	1.0041192	1.0353349	1.0346334	1.0680342	1.0750695				
standard_error	0.04119575	0.6166694	0.6986288	0.7153321	0.752788		0.0608333	0.0846357	0.1208244	0.1256557	0.1700872		0.0359884	0.0395718	0.0402604	0.04000562	0.0382495	0	0.0120158	0.0311924	0.030459	0.0357437	0.0364514				
n	18	18	18	18	18		24	24	24	24	24		23	23	23	23	23	23	6	6	6	6	6	6			
standardDev	0.17477877	2.6163066	2.964031	3.0348973	3.1938092		0.2980211	0.4146285	0.5919161	0.6155846	0.8332537		0.1725943	0.1897795	0.1930819	0.1921029	0.1834382	0	0.0294326	0.0764054	0.0746089	0.0875539	0.0892873				
median	1.24072662	3.5087465	4.0297952	4.2789904	4.781108		1.0984043	0.9910408	0.9959771	1.0320569	1.0145438		1.0104538	0.9689885	1.0080894	1.0019789	0.9856886	0	1.0129771	1.0656697	1.0520633	1.0755531	1.0889921				
variance	1.30547617	6.8490604	8.7854796	9.2106034	10.200417		0.0888166	0.1719168	0.3503646	0.3789444	0.6943118		0.871868	0.6448058	0.3196358	0.4038957	0.080163	0	0.0008663	0.0058378	0.0055665	0.0076551	0.0079722				
skewness	NaN	0.7530691	0.6389153	0.476787	0.3241089	0.2562234	NaN	1.965081	1.1928257	1.2734688	1.1184102	NaN		0.871868	0.6448058	0.3196358	0.4038957	0.080163	NaN	-0.864216	-1.276824	-0.29633	0.0725815	-0.325631			
kurtosis	NaN	2.4483479	2.4002805	1.9454419	1.7766584	1.7011546	NaN	5.9973711	3.0482842	3.3477887	2.9348639	3.8957485	NaN	3.6665077	2.2833994	2.1066694	2.1384224	2.0482884	NaN	2.4130508	3.154621	1.6114242	1.8095856	2.048169			

FIG 3.2B

	Mgel0'	Mgel10'	Mgel20'	Mgel30'	Mgel40'	Mgel50'	MCm0'	MCm10'	MCm20'	MCm30'	MCm40'	MCm50'	MC0'	MC10'	MC20'	MC30'	MC40'	MC50'	G0'	G10'	G20'	G30'	G40'	G50'	
Mgel0'	1																								
Mgel10'	0.0046255	1																							
Mgel20'	0.0041853	0.6238298	1																						
Mgel30'	0.0015547	0.3345251	0.4963035	1																					
Mgel40'	0.0005001	0.1172991	0.1838787	0.4197908	1																				
Mgel50'	0.0005969	0.0904985	0.1736568	0.5168955	0.8867848	1																			
MCm0'	0.0005209	1.20E-06	5.50E-06	1.28E-06	1.55E-06	1.46E-06	1																		
MCm10'	0.1304921	1.55E-05	2.32E-05	9.74E-06	6.43E-06	3.96E-06	0.1054958	1																	
MCm20'	0.315364	0.0018472	0.0015536	0.0005464	0.0001178	0.0001306	0.1608291	0.7570654	1																
MCm30'	0.4306937	0.0091768	0.0082048	0.003759	0.0011923	0.001303	0.026629	0.4831655	0.584736	1															
MCm40'	0.2272489	0.002702	0.0036081	0.0009954	0.0004102	0.0001521	0.1608064	0.7965708	0.9096973	0.5102698	1														
MCm50'	0.3805297	0.0070524	0.0051752	0.0020144	0.0003731	0.0004313	0.307357	0.6724869	0.942466	0.5226417	0.9096875	1													
MC0'	0.7826535	0.0002231	0.0001066	6.17E-05	3.13E-05	1.46E-05	0.0018208	0.144884	0.400536	0.5727387	0.3600276	0.6320287	1												
MC10'	0.2585513	1.08E-05	2.21E-05	8.46E-06	8.46E-06	6.45E-06	0.0103219	0.6781247	0.9490884	0.85644	0.8066058	0.4099414	0.6683318	1											
MC20'	0.5721679	4.40E-05	3.93E-05	2.79E-05	1.22E-05	6.62E-06	0.0073234	0.9745312	0.7738452	0.9660481	0.8175441	0.616975	0.6683318	0.8175441	1										
MC30'	0.8232733	0.0001813	0.0001067	6.17E-05	4.41E-05	1.75E-05	0.0005217	0.186994	0.4824751	0.647266	0.4563106	0.616975	0.947445	0.4099703	0.509769	1									
MC40'	0.8029044	0.0002011	0.0001124	4.40E-05	3.51E-05	1.08E-05	0.0011275	0.1905741	0.502576	0.7095366	0.4692667	0.6320484	0.947445	0.4099703	0.6683029	0.8604749	1								
MC50'	0.5198014	4.40E-05	4.16E-05	3.59E-05	9.38E-06	8.47E-06	0.0120171	0.3435434	0.6396286	0.9494913	0.6020604	0.9830207	0.6210359	0.6133106	0.6608386	0.6603541	1								
G0'	0.0003594	0.0003594	0.0015383	0.0003605	0.0007588	0.0010828	0.051783	0.0257348	0.0969795	0.075482	0.0293457	0.1022744	0.0028012	0.0008339	0.0046957	0.0002785	0.0003421	0.0055541	1						
G10'	0.0004626	0.0003594	0.0007588	0.0003605	0.0004639	0.0005946	0.020957	0.031136	0.0147498	0.0033892	0.0158659	0.0656517	0.001122	0.0006262	0.0017855	0.0002785	0.0003421	0.0013564	0.1385281	1					
G20'	0.0003594	0.0003594	0.0009644	0.0003605	0.0004639	0.0007588	0.0182563	0.0102406	0.0583768	0.0059807	0.0240472	0.0919434	0.0011172	0.0006262	0.0025609	0.0002257	0.0002425	0.1688312	0.5692641	0.0303003	0.0238095	1			
G30'	0.0045977	0.0004639	0.001542	0.0005962	0.0009668	0.001542	0.687318	0.0919434	0.1694063	0.0550112	0.1260132	0.2878384	0.0090153	0.0122766	0.0254101	0.0033443	0.0047008	0.0165842	0.1515152	0.0303003	0.0238095	0.0303003	1		
G40'	0.0056424	0.0004626	0.0012205	0.0009664	0.0012205	0.0012205	0.9793066	0.1260553	0.1775017	0.1022362	0.2036376	0.3374142	0.0089814	0.0333873	0.0254282	0.0055541	0.0070833	0.0221114	0.0865801	0.1168831	0.0541126	0.09090909	0.09090909	1	
G50'	0.0007568	0.0003594	0.0015383	0.0003605	0.0005946	0.0013677	0.1463963	0.0257348	0.0969795	0.0118976	0.0549301	0.1394558	0.0046957	0.0036294	0.007684	0.0006922	0.0010186	0.0076915	0.8917749	0.1233766	0.1255411	0.2900433	0.2337662	1	
mean	0.7172222	0.513	0.4932778	0.4630556	0.4257778	0.4195	0.866	0.8011667	0.7473333	0.7174583	0.745375	0.724125	0.7480435	0.7699043	0.7494348	0.7538696	0.7739608	0.8323333	0.9385	0.9371667	0.9126667	0.9071667	0.927		
standard_error	0.0469009	0.0432443	0.0448777	0.0484941	0.0487665	0.0459429	0.0239111	0.0295679	0.0458254	0.0530563	0.0488792	0.049315	0.0301236	0.0262288	0.0294413	0.0306803	0.0300706	0.0279473	0.0024989	0.0058694	0.0027254	0.0100918	0.0126027	0.0061698	
n	18	18	18	18	18	18	18	18	24	24	24	24	24	24	24	23	23	23	23	23	23	23	6	6	6
standardDev	0.1989838	0.1834686	0.1903998	0.205743	0.2068988	0.1949191	0.1171398	0.1448527	0.2244976	0.2599217	0.2394582	0.2415933	0.1444675	0.1257891	0.1411957	0.1471375	0.1442133	0.1340304	0.006121	0.0143771	0.0066758	0.0247198	0.0308702	0.0151129	
median	0.7465	0.5115	0.502	0.3985	0.3605	0.3605	0.3945	0.9175	0.8735	0.863	0.87	0.8705	0.769	0.844	0.773	0.8	0.8	0.8	0.932	0.9435	0.9375	0.916	0.913	0.934	
variance	0.0395945	0.0336612	0.0362521	0.0423302	0.0428071	0.0379934	0.0137217	0.0220823	0.0503992	0.0675593	0.0573402	0.0583673	0.0208709	0.0158229	0.0199362	0.0216494	0.0207975	0.0179642	3.75E-05	0.0002067	4.46E-05	0.0006111	0.000953	0.0002284	
skewness	-0.908735	0.2332523	0.4334169	0.6432486	0.84719	0.9884593	-2.36455	-0.773889	-0.806669	-0.888541	-0.890788	-0.495777	-0.40861	-0.553667	-0.409893	-0.448936	-0.411556	-0.323077	-0.601433	-1.144789	-0.624256	-0.778349	-0.152727	-1.388876	
kurtosis	2.5307187	3.3141476	2.9193999	3.2095485	4.1196369	7.4093295	2.1463649	2.1260812	1.5820133	2.2248167	2.1069645	2.1427917	1.9325629	1.7602542	1.6722673	2.4644445	2.9548324	2.29531	2.4990368	1.8634832	3.366138				

FIG 3.2C

	Mgel0'	Mgel10'	Mgel20'	Mgel30'	Mgel40'	Mgel50'	MCm0'	MCm10'	MCm20'	MCm30'	MCm40'	MCm50'	MC0'	MC10'	MC20'	MC30'	MC40'	MC50'	G0'	G10'	G20'	G30'	G40'	G50'	
Mgel0'	1																								
Mgel10'	0.3112989	1																							
Mgel20'	0.3506451	0.8618558	1																						
Mgel30'	0.2292302	0.4963589	0.5166026	1																					
Mgel40'	0.1065985	0.132882	0.149993	0.8370636	1																				
Mgel50'	0.0875261	0.148993	0.1591554	0.6924868	0.9747586	1																			
MCm0'	0.0488095	0.8289432	0.5760052	0.7997731	0.1992702	0.3032101	1																		
MCm10'	0.0065326	0.3405117	0.5503003	0.7797818	0.4087659	0.5168911	0.0711278	1																	
MCm20'	0.0599348	0.5672689	0.7410268	0.9291014	0.3944234	0.4687496	0.9014987	0.3024177	1																
MCm30'	0.0229142	0.4233343	0.5760206	0.828895	0.4845645	0.6291303	0.307265	0.6724786	0.6875344	1															
MCm40'	0.0244784	0.2743766	0.4533478	0.8091865	0.6201339	0.7314859	0.4896467	0.7570718	0.4453092	0.8608474	1														
MCm50'	0.0207181	0.1820674	0.2914665	0.6472881	0.7700567	0.8888212	0.3073044	0.9835468	0.5159118	0.6649799	0.9917728	1													
MC0'	0.0065483	0.2641293	0.4540351	0.8664146	0.3245563	0.4863526	0.0704339	0.8648048	0.3544829	0.6204099	0.8895581	0.9406228	1												
MC10'	0.0099765	0.1243058	0.1637679	0.5369663	0.4698887	0.703238	0.0013083	0.2920742	0.0671565	0.150826	0.2548336	0.3886618	0.3794981	1											
MC20'	0.0012897	0.0926758	0.1522021	0.5544477	0.4540154	0.6084452	0.0033095	0.186943	0.0489678	0.1478002	0.2092071	0.3495036	0.3282282	0.9299639	1										
MC30'	0.0027449	0.11090316	0.2169198	0.8233036	0.4229895	0.5544649	0.0489808	0.5026131	0.2129867	0.377126	0.5727165	0.7495448	0.6133325	0.7500431	0.8261059	1									
MC40'	0.0010226	0.1411495	0.3577911	0.6935023	0.4079039	0.5721344	0.0066443	0.558353	0.1697374	0.3600415	0.4958059	0.7738452	0.6288142	0.6924513	0.6182887	0.9824698	1								
MC50'	0.000453	0.0761876	0.1412361	0.5722013	0.4700274	0.6457093	0.001462	0.209194	0.0655589	0.1334041	0.2375286	0.4628086	0.356131	0.9212411	0.8951209	0.660364	0.5678411	1							
G0'	0.2713321	0.9734088	0.738828	0.8676323	0.3337107	0.4432797	0.8968451	0.31119492	1																
G10'	0.1717298	0.9203443	0.6647726	0.9734088	0.3681203	0.526516	0.7753743	0.2876775	0.9793066	0.5337384	0.697318	0.5860415	0.2470595	0.0525146	0.0357107	0.2257577	0.1247018	0.0434426	0.6991342	1					
G20'	0.6647726	0.7641772	0.7138677	0.7138677	0.3014479	0.3681203	0.3118954	0.102389	0.3920192	0.2986508	0.2538584	0.2876238	0.1459889	0.0220976	0.022114	0.0755881	0.0594254	0.0254643	0.6233766	0.6348485	1				
G30'	0.14238	1	0.9734088	0.9734088	0.4432797	0.526516	0.7359968	0.5167837	0.9173563	0.7754959	0.79593849	0.69735	0.4350062	0.1696864	0.19660412	0.2937895	0.2056888	0.1697916	0.8528139	0.6991342	0.9372294	0.3939394	1		
G40'	0.2713321	0.9203443	0.8155026	0.8155026	0.4046568	0.4046568	0.4839273	0.9379961	0.39223	0.8153763	0.6040458	0.6592494	0.4366357	0.3461065	0.0846904	0.0898647	0.2058005	0.1614204	0.080163	0.8181818	1				
G50'																									
mean	0.8979444	0.9318889	0.9421667	1.2122222	1.3435556	1.3772778	1.08475	1.1975833	1.2180417	1.27075	1.3050417	1.3832917	1.1666087	1.2073043	1.2012174	1.098	1.084	1.0786667	1.0726667	1.104	1.0923333				
standart_error	0.0752838	0.0970621	0.1050425	0.1822022	0.2194102	0.2282347	0.0119087	0.059248	0.0870367	0.1017363	0.1353879	0.0300243	0.0384277	0.0250785	0.0362692	0.0299198	0.0299032	0.0250785	0.0164033	0.0127976	0.0236892	0.0294686	0.0314141		
n	18	18	18	18	18	18	24	24	24	24	24	24	24	24	24	23	23	23	23	23	23	6	6	6	6
standartDev	0.3194019	0.4117998	0.4456574	0.7730185	0.9308785	0.9683179	0.0583403	0.2902546	0.4263911	0.5675494	0.4984038	0.6632626	0.1439914	0.1842929	0.1751895	0.1565322	0.1434901	0.1434107	0.0614296	0.0401796	0.0313475	0.0580264	0.0721831	0.0769485	
variance	0.1020176	0.169579	0.1986105	0.5975576	0.8665348	0.9376396	0.0034036	0.0842477	0.1818093	0.3221123	0.2484064	0.4399173	0.0207335	0.0339639	0.0306914	0.0245023	0.0205894	0.0205666	0.0037736	0.0016144	0.0009827	0.0033671	0.0052104	0.0059211	
skewness	-0.754379	-0.597619	-0.496768	0.3577768	0.8244717	0.7497403	3.0498946	3.1482284	3.642802	3.6874762	2.4387507	2.6883585	0.9687775	1.442077	1.5941144	0.4520437	0.8988692	0.5151769	-0.027219	0.3457885	-0.26148	0.9669505	0.6275534	0.8208523	
kurtosis	2.0962612	1.9353544	1.887228	2.125666	3.8078321	2.9119332	13.668878	12.958045	16.17705	16.269705	8.6051421	10.109721	2.7012463	4.2493299	5.0586699	1.707807	2.5611285	1.7823203	1.449131	1.7043407	2.034718	2.5800877	1.9516277	2.7727028	

FIG 3.2D

A_Mgel'	A_MCm'	A_MC'	'A_G'	A_IR_Mgel'	A_IR_MCm'	A_IR_MC'	'A_IR_G'
1							
0,03646265	1						
5,03E-29	1,83E-18	1					
1,70E-30	3,09E-25	0,000375796	1				
7,38E-07	0,005288313	9,14E-08	1,23E-12	1			
0,000453638	0,274568679	7,07E-19	3,07E-25	0,040306745	1		
4,55E-14	9,84E-08	0,000141375	7,11E-11	0,03103024	1,14E-06	1	
7,42E-40	1,19E-31	1,74E-07	0,125714902	5,80E-18	1,53E-33	9,82E-16	1

	A_Mgel'	A_MCm'	A_MC'	'A_G'	A_IR_Mgel'	A_IR_MCm'	A_IR_MC'	'A_IR_G'
mean	784,5323501	683,8441915	383,5480856	245,1461553	582,6123513	642,914865	474,999519	231,3895257
standart_error	30,87091205	42,58541218	32,3121693	6,583132115	32,76978237	27,79513397	26,40758068	5,226750713
n	283	145	213	97	185	255	182	130
standartDev	519,3291237	512,7962684	471,5805856	64,8363321	445,7172285	443,8526957	356,2577406	59,59412716
median	690,3523562	568,8543883	266,8935896	234,4649657	467,0159317	546,569963	355,4502552	226,1185598
variance	269702,7387	262960,0129	222388,2487	4203,74996	198663,8478	197005,2155	126919,5778	3551,459992
skewness	1,393663197	3,360841143	9,193642128	1,743736407	1,710607303	1,511563077	1,960376481	0,725347273
kurtosis	5,90844992	21,90115982	111,1068206	8,969548609	6,439673126	5,293376714	7,132156649	4,06974266

FIG 3.2E

	circ_Mgel'	circ_MCm'	circ_MC'	'circ_G'	circ_IR_Mgel'	circ_IR_MCm'	circ_IR_MC'	circ_IR_G'	
circ_Mgel'	1								
circ_MCm'	2,31E-12	1							
circ_MC'	4,72E-42	2,14E-12	1						
'circ_G'	1,29E-39	1,57E-21	9,94E-05	1					
circ_IR_Mgel'	1,68E-08	0,616740454	1,84E-11	3,24E-17	1				
circ_IR_MCm'	3,62E-21	0,089580259	4,71E-11	5,59E-21	0,059271179	1			
circ_IR_MC'	2,16E-21	0,017276268	3,20E-07	9,96E-16	0,01295879	0,331077799	1		
circ_IR_G'	5,77E-54	1,12E-30	2,69E-19	8,54E-10	4,32E-32	4,64E-36	1,90E-31	1	
mean		circ_Mgel'	circ_MCm'	circ_MC'	'circ_G'	circ_IR_Mgel'	circ_IR_MCm'	circ_IR_MC'	circ_IR_G'
standart_error		0,396010601	0,54522069	0,72856338	0,852907216	0,542108108	0,582427451	0,611098901	0,894223077
n		0,013141601	0,017970278	0,014234434	0,007431807	0,020237568	0,014122987	0,017011962	0,007394927
standartDev		283	145	213	97	185	255	182	130
median		0,221075955	0,216390801	0,207744723	0,073194815	0,275260685	0,22552602	0,229503912	0,08431514
variance		0,336	0,497	0,807	0,873	0,504	0,556	0,575	0,9225
skewness		0,048874578	0,046824979	0,04315787	0,005357481	0,075768445	0,050861986	0,052672045	0,007109043
kurtosis		0,846590997	0,468787606	-0,782087885	-0,817162299	0,057151195	0,093988382	-0,022683444	-3,200041044
		2,766015431	2,137913204	2,282942311	2,64319361	1,603035807	1,6484186172	1,648415209	14,74980753

FIG 3.2F

	AR_Mgel'	AR_MCm'	AR_MC'	'AR_G'	AR_IR_Mgel'	AR_IR_MCm'	AR_IR_MC'	'AR_IR_G'
AR_Mgel'	1							
AR_MCm'	0,061247928	1						
AR_MC'	4,31E-24	1,19E-12	1					
'AR_G'	2,36E-35	2,13E-25	1,12E-10	1				
AR_IR_Mgel'	0,015751873	0,583996906	2,09E-09	6,94E-20	1			
AR_IR_MCm'	9,92E-05	0,136397545	2,20E-11	5,95E-27	0,507314165	1		
AR_IR_MC'	6,63E-07	0,006484529	0,000136642	7,41E-15	0,031415463	0,068907451	1	
'AR_IR_G'	1,17E-43	6,05E-30	2,57E-15	0,154736229	4,13E-25	3,59E-34	3,05E-19	1

	AR_Mgel'	AR_MCm'	AR_MC'	'AR_G'	AR_IR_Mgel'	AR_IR_MCm'	AR_IR_MC'	'AR_IR_G'
mean	3,134671378	2,584365517	1,607380282	1,128443299	2,949216216	2,503556863	2,178587912	1,137669231
standart_error	0,151557696	0,142996755	0,063264545	0,011501484	0,2052108	0,124294458	0,107091936	0,017447925
n	283	145	213	97	185	255	182	130
standartDev	2,549595076	1,721908953	0,923315642	0,113276484	2,791168642	1,984823322	1,444749197	0,198936957
median	2,188	1,963	1,235	1,1	1,887	1,692	1,572	1,0765
variance	6,500435051	2,964970442	0,852511775	0,012831562	7,790622388	3,939523618	2,087300244	0,039575913
skewness	2,217793238	1,508695058	2,752046482	1,815094822	2,55811929	2,115794104	1,631841523	3,993120583
kurtosis	9,057607318	4,700020967	11,25535936	6,125244433	10,59785875	7,538166448	5,909108384	22,34492675

FIG 3.2G

	Mgels'	MCmS'	MCS'	IRMgels'	IRMCmS'	IRMCS'
Mgels'	1					
MCmS'	1,76E-05	1				
MCS'	1,16E-08	0,000736	1			
IRMgels'	0,5823194	0,0007058	8,89E-08	1		
IRMCmS'	2,87E-05	0,8690032	4,12E-05	0,0006244	1	
IRMCS'	0,0001686	0,6254264	1,26E-05	0,0012583	0,8564523	1

	Mgels'	MCmS'	MCS'	IRMgels'	IRMCmS'	IRMCS'
mean	0,48337	0,18219	0,08763	0,51338	0,19237	0,21559
standart_error	0,0565456	0,0228281	0,0061025	0,1099981	0,0237007	0,032907
n	20	22	29	15	24	23
standartDev	0,2528796	0,1070732	0,0328628	0,4260207	0,1161092	0,1578162
median	0,423867	0,1524539	0,0837999	0,3541015	0,1666373	0,1487383
variance	0,0639481	0,0114647	0,00108	0,1814936	0,0134813	0,0249059
skewness	0,6887526	0,7036154	0,6184222	1,479847	1,2218396	1,443478
kurtosis	2,83751	2,6732413	2,5718397	3,9542464	4,1165445	4,0698919

FIG 3.2H

	Mgelp'	MCmpP'	MCP'	IRMgelp'	IRMCmpP'	IRMCP'
Mgelp'	1					
MCmpP'	0,3988514	1				
MCP'	0,0973447	0,0059926	1			
IRMgelp'	0,4334314	0,768852	0,0353307	1		
IRMCmpP'	0,6289611	0,1626051	0,16611	0,179486	1	
IRMCP'	0,6878589	0,1840829	0,184659	0,3099257	0,9237061	1

	Mgelp'	MCmpP'	MCP'	IRMgelp'	IRMCmpP'	IRMCP'
mean	0,3261225	0,3813989	0,2206074	0,4055438	0,2921564	0,3022702
standart_error	0,0479925	0,0464259	0,0251874	0,070464	0,0378494	0,0413946
n	20	22	29	15	24	23
standartDev	0,214629	0,2177568	0,1356383	0,2729059	0,1854234	0,1985216
median	0,3118452	0,3515034	0,2084409	0,4218423	0,2787826	0,2339968
variance	0,0460656	0,047418	0,0183977	0,0744777	0,0343818	0,0394108
skewness	0,6972501	0,6802757	0,5573317	0,3403397	1,1746042	0,643382
kurtosis	3,0189941	2,5741915	2,2830501	2,1991027	4,4575295	2,3611775

FIG 3.12D

	MBCCd5'	BBCCd5'	LBCCd5'	MBCCMCd5'	BBCCMCd5'	LBCCMCd5'
MBCCd5'	1					
BBCCd5'	0,028571429	1				
LBCCd5'	0,885714286	0,028571429	1			
MBCCMCd5'	0,114285714	0,028571429	0,171428571	1		
BBCCMCd5'	0,628571429	0,028571429	0,342857143	0,257142857	1	
LBCCMCd5'	1	0,028571429	1	0,114285714	0,428571429	1

	MBCCd5'	BBCCd5'	LBCCd5'	MBCCMCd5'	BBCCMCd5'	LBCCMCd5'
mean	7,25	16	7	2,25	5,25	7,25
standart_error	1,931105038	1,290994449	1,354006401	1,652018967	2,015564437	1,030776406
n	4	4	4	4	4	4
standartDev	3,862210075	2,581988897	2,708012802	3,304037934	4,031128874	2,061552813
median	7,5	16	6	1	4	7,5
variance	14,916666667	6,666666667	7,333333333	10,916666667	16,25	4,25
skewness	-0,097709392	0	1,046621698	0,900382043	0,848320697	-0,115317183
kurtosis	1,212103243	1,64	2,26446281	2,089680089	2,070769231	1,152249135

FIG 3.146-H

	NmBCcd1'	NmBCcd3'	NmBCcd5'	NmBCCMcd1'	NmBCCMcd3'	NmBCCMcd5'	NmMcd1'	NmMcd3'	NmMcd5'	NcBCCd1'	NcBCCd3'	NcBCCd5'	NcBCCMcd1'	NcBCCMcd3'	NcBCCMcd5'	NcMcd1'	NcMcd3'	NcMcd5'
NmBCcd1'	1																	
NmBCcd3'	0.006993007	0.020668221	1															
NmBCcd5'	0.000621601	0.0003108	0.0001554	1														
NmBCCMcd1'	0.028127428	0.020668221	0.00021601	0.082983683	1													
NmBCCMcd3'	0.328205128	0.573737374	0.002952603	0.01087801	0.04988345	1												
NmBCCMcd5'	0.0003108	0.0001554	0.0001554	0.14763015	0.0001554	0.0001554	1											
NmMcd1'	0.000621601	0.0001554	0.0001554	0.959129759	0.028127428	0.0001554	0.038137438	1										
NmMcd3'	0.002952603	0.0001554	0.0001554	0.328205128	0.328205128	0.082983683	0.082983683	0.082983683	1									
NmMcd5'	0.000165824	0.000100839	0.000100839	0.408405541	0.00533144	0.009252446	0.009252446	0.009252446	0.009252446	1								
NcBCCd1'	0.060993937	0.000268834	0.000129542	0.070840479	0.000334481	0.003334481	0.003334481	0.003334481	0.003334481	9.59E-05	1							
NcBCCd3'	0.690599165	0.002435487	0.000340448	0.00533144	0.133533481	0.000268834	0.000340448	0.000340448	0.000340448	0.01849494	0.002120795	1						
NcBCCd5'	0.000669862	9.94E-05	9.94E-05	0.645746486	0.025279443	9.94E-05	0.736042953	0.56039133	0.133195588	0.558956279	0.052260791	0.509538756	1					
NcBCCMcd1'	0.481290609	0.150129211	0.000540367	0.007725887	0.408405541	0.312296735	0.001052168	0.002977936	0.029710983	9.59E-05	0.052260791	0.509538756	0.000317469	1				
NcBCCMcd3'	0.000100839	0.001612048	0.481290609	0.000100839	0.000165824	0.000211513	0.000100839	0.000100839	0.000100839	1.54E-06	1.54E-06	1.53E-06	3.25E-06	1				
NcBCCMcd5'	0.000100839	0.000100839	0.000100839	0.602703582	0.01104267	0.000100839	0.342530457	0.018391822	0.509538756	8.20E-05	6.67E-06	0.924905123	1.54E-06	1.54E-06	1			
NcMcd1'	0.443994376	0.021653213	0.000429693	0.00533144	0.209546836	0.168253317	0.000677151	0.001384911	1.89E-05	0.00983176	0.63750113	6.96E-05	0.835784126	1.86E-06	2.24E-05	1		
NcMcd3'	0.000100488	0.005321482	0.015546257	0.000100488	0.000100488	0.000100488	0.000100488	0.000100488	0.000100488	1.54E-06	1.54E-06	1.54E-06	0.000973475	1.54E-06	3.89E-06	1		
NcMcd5'																		
mean	NmBCcd1'	NmBCcd3'	NmBCcd5'	NmBCCMcd1'	NmBCCMcd3'	NmBCCMcd5'	NmMcd1'	NmMcd3'	NmMcd5'	NcBCCd1'	NcBCCd3'	NcBCCd5'	NcBCCMcd1'	NcBCCMcd3'	NcBCCMcd5'	NcMcd1'	NcMcd3'	NcMcd5'
standart_error	3.273585615	5.780603301	9.508180551	1.567035389	3.102977165	5.222295183	1	1.328798547	1.806999173	1.000000744	2.443911036	3.444221917	1.243071531	4.119962873	9.575438063	1.111980185	3.756197785	8.059450605
n	0.409231196	0.748388274	0.862918891	0.440348463	0.881896225	0.709211023	0.225463672	0.199433208	0.211538579	0.155373776	0.237170721	0.294843926	0.222966206	0.610764965	0.295430835	0.131035648	0.407655825	0.299594892
standartDev	1.157480614	2.116761693	2.440703197	1.245493622	2.494379203	2.005951693	0.637707566	0.564082295	0.598321456	0.621495104	0.940882886	1.179375705	0.919848238	2.443059858	1.181723338	0.524142592	1.630623301	1.198194368
median	2.945773479	5.511596827	9.711146723	1.041568074	2.19084866	4.504914694	0.813831726	1.039496902	1.766478256	1.012308236	2.3753347	3.41896433	0.906484402	3.622434296	9.428186078	1.07532815	3.903602357	8.157863397
variance	1.339761371	4.480680064	5.957032096	1.551254362	6.221927608	4.023842196	0.40667094	0.318188836	0.357988564	0.386256165	0.899999218	1.390927054	0.846120781	5.968541472	1.396470048	0.274725457	2.65893235	1.4356669745
skewness	0.720238151	1.178218138	-1.299129721	0.773230078	1.384844414	0.656068323	0.289088433	0.674418357	0.246003549	0.349328138	0.438618696	-0.114387791	0.396385314	0.25278179	0.15320739	-0.032350767	0.240456137	0.190652661
kurtosis	2.627199245	3.841091425	4.087749941	2.1191517912	3.796534035	2.048872533	1.717250097	1.75172632	1.722112765	2.629737785	2.749339836	1.71634717	1.696003268	1.751244805	2.653053804	1.455846361	3.329122131	2.599372557

FIG 3.15B

	MC'	BSA'	EGF'
MC'	1		
BSA'	0,0015456	1	
EGF'	5,25E-10	0,0004002	1

	MC'	BSA'	EGF'
mean	0,5750816	0,4766515	0,3787662
standart_error	0,0160108	0,0209006	0,0150515
n	27	35	45
standartDev	0,0831943	0,1236496	0,1009685
median	0,5764692	0,4546741	0,3664279
variance	0,0069213	0,0152892	0,0101946
skewness	-0,209345	-0,099442	-0,134398
kurtosis	3,4603487	2,3929511	2,8172816